IMMUNOLOGY

CD47 halts *Ptpn6*-deficient neutrophils from provoking lethal inflammation

Lalita Mazgaeen[1,2,3], Matthew Yorek[1,2], Saurabh Saini[1,2], Peter Vogel[4], David K. Meyerholz[5], Thirumala-Devi Kanneganti[6], Prajwal Gurung[1,2,3,7,8]*

Mice with SHP1 proteins, which have a single amino acid substitution from tyrosine-208 residue to asparagine (hereafter *Ptpn6*^{spin} mice), develop an autoinflammatory disease with inflamed footpads. Genetic crosses to study CD47 function in *Ptpn6*^{spin} mice bred *Ptpn6*^{spin} × *Cd47*$^{-/-}$ mice that were not born at the expected Mendelian ratio. *Ptpn6*^{spin} bone marrow cells, when transferred into lethally irradiated *Cd47*-deficient mice, caused marked weight loss and subsequent death. At a cellular level, *Ptpn6*-deficient neutrophils promoted weight loss and death of the lethally irradiated *Cd47*$^{-/-}$ recipients. We posited that leakage of gut microbiota promotes morbidity and mortality in *Cd47*$^{-/-}$ mice receiving *Ptpn6*^{spin} cells. Colonic cell death and gut leakage were substantially increased in the diseased *Cd47*$^{-/-}$ mice. Last, IL-1 blockade using anakinra rescued the morbidity and mortality observed in the diseased *Cd47*$^{-/-}$ mice. These data together demonstrate a protective role for CD47 in tempering pathogenic neutrophils in the *Ptpn6*^{spin} mice.

INTRODUCTION

Neutrophilic dermatosis is a rare disorder that includes a spectrum of diseases such as Sweet's syndrome (*1*), subcorneal pustular dermatosis (*2*), and pyoderma gangrenosum (*3*), all of which are hallmarked by skin lesions packed with neutrophils (*4*). Given the rarity of these disorders, understanding the etiology and biology of these diseases has been challenging; thus, most treatment strategies are limited to the use of strong immunosuppressive (*5*). Genome-wide association studies of humans affected with neutrophilic dermatosis have found variations in the *PTPN6* gene, suggesting a potential link of this particular gene to the disease (*6*). In 2008, Croker *et al.* (*7*) generated C57BL/6J (B6) mice with a hypomorphic point mutation in the *Ptpn6* gene using *N*-ethyl-*N*-nitrosourea mutagenesis, which resulted in tyrosine-208 to asparagine amino acid substitution in the *Ptpn6*-encoded SHP1 protein. Because of the resulting mutated SHP1 protein, these mice have reduced phosphatase activity and develop spontaneous inflammation of the footpads, and thus were aptly named *Ptpn6*^{spin} mice (*7*). In addition, an independent mouse line with reduced SHP1 activity due to a B2 element insertion in exon 6 of the *Ptpn6* gene also developed similar spontaneous inflammation of the footpads (*8*). The inflamed skin lesions of the footpads from *Ptpn6*^{spin} mice are replete with neutrophils and closely mimic the clinical presentations of lesions from patients suffering from neutrophilic dermatosis disorders, providing further confirmation for a regulatory role for SHP1 in neutrophilic dermatosis (*9*).

Genetic ablation studies have been successful at elucidating the molecular pathways governing the inflammatory cascades leading to footpad inflammation in *Ptpn6*^{spin} mice (*7*, *9*–*15*). Previous studies have shown that *Ptpn6*^{spin} mice lacking interleukin-1α (IL-1α), but not IL-1β, were completely protected from this autoinflammatory syndrome, suggesting a crucial role for IL-1α in driving this disease (*9*). Mechanistically, IL-1α produced by radioresistant cells in the footpad is crucial for recruiting pathogenic *Ptpn6*^{spin} neutrophils that then drive the autoinflammatory disease (*12*, *16*). IL-1α signaling in neutrophils promotes SYK-dependent MyD88 phosphorylation and subsequent recruitment of the RIPK1/TAK1 signaling platform, which promotes neutrophil-mediated autoinflammation and disease in *Ptpn6*^{spin} mice (*12*). Given the absolute requirement of IL-1α in the progression of neutrophilic dermatosis in these mouse models, an IL-1α inhibitor (bermekimab) is currently in clinical trials for the treatment of pyoderma gangrenosum (ClinicalTrials.gov identifier no., NCT01965613) (*17*).

Integrins have long been proposed to regulate IL-1α expression via direct activation of the mitogen-activated protein kinase (MAPK) pathway (*18*, *19*). Integrins, specifically ITGB3, regulate IL-1α production during viral infection (*20*). To gain further insight into the mechanisms that regulate IL-1α in *Ptpn6*^{spin} mice, we hypothesized that ITGB3 promotes aberrant IL-1α expression and production in *Ptpn6*^{spin} mice. However, *Ptpn6*^{spin} mice deficient in ITGB3 still develop footpad inflammation (*12*). In this study, we focused our attention on CD47, an integrin-associated protein (*21*), and examined the role of CD47 in *Ptpn6*^{spin} mice. CD47 is a "don't eat me signal" that is ubiquitously present on all cells, including cancerous cells (*22*). Hence, CD47 has been targeted in several cancer studies with great success (*23*–*27*), and clinical trials targeting CD47 are currently in progress [NCT02678338 (*28*), NCT02663518 (*29*), NCT02216409 (*30*), NCT02953782, and NCT02953509].

Thus, we hypothesized that blocking CD47 may ameliorate the spontaneous neutrophilic inflammatory disease observed in *Ptpn6*^{spin} mice. Our results show that CD47 is required for the survival of *Ptpn6*^{spin} mice and that radioresistant CD47 is critical for this survival. In the absence of radioresistant CD47, pathogenic *Ptpn6*^{spin} cells provoke a systemic inflammatory disease that

[1]Inflammation Program, University of Iowa, Iowa City, IA 52242, USA. [2]Department of Internal Medicine, University of Iowa, Iowa City, IA 52242, USA. [3]Interdisciplinary Graduate Program in Human Toxicology, University of Iowa, Iowa City, IA 52242, USA. [4]Animal Resources Center and the Veterinary Pathology Core, St. Jude Children's Research Hospital, Memphis, TN 38105, USA. [5]Department of Pathology, University of Iowa, Iowa City, IA 52242, USA. [6]Department of Immunology, St. Jude Children's Research Hospital, Memphis, TN 38105, USA. [7]Immunology Graduate Program, University of Iowa, Iowa City, IA 52241, USA. [8]Center for Immunology and Immune-Based Disease, University of Iowa, Iowa City, IA 52241, USA.
*Corresponding author. Email: prajwal-gurung@uiowa.edu

results in multiorgan damage, wasting, and death in mice. We further show that *Ptpn6* deficiency in neutrophils is sufficient to provoke the lethal inflammation in *Cd47*-deficient mice. Mechanistically, the absence of CD47 in the radioresistant compartment results in *Ptpn6*^{spin} cell–driven colonic tissue damage and systemic leakage of gut bacterial products, which ultimately presents as lymphopenia in these mice. Last, we demonstrate that IL-1 signaling is critical for this pathogenic outcome as neutralization of IL-1 signaling by anakinra prevents morbidity and mortality provoked by *Ptpn6*^{spin} cells in CD47-deficient recipient mice. In conclusion, we report an unexpected regulatory role for CD47 in ameliorating lethal systemic wasting disease in *Ptpn6*^{spin} mice.

RESULTS

CD47 is required for survival of *Ptpn6*^{spin} mice

Ptpn6^{spin} mice develop spontaneous footpad inflammation hallmarked by neutrophilic infiltrates (*9*, *13*–*15*). Given the severe footpad inflammation observed in *Ptpn6*^{spin} mice, we first asked whether these mice were born at expected Mendelian ratio. To this end, we bred *Ptpn6*$^{spin/+}$ mice together and genotyped the pups born to these HT breeders. As expected, approximately 25% of the pups born to the *Ptpn6*$^{spin/+}$ breeders were homozygous for the spin mutation (fig. S1). As demonstrated previously, these *Ptpn6*^{spin} mice also develop spontaneous footpad inflammation at around 6 to 16 weeks of age (fig. S1). To study the potential role of CD47 in *Ptpn6*^{spin}-mediated disease, we generated *Cd47*$^{-/-}$ × *Ptpn6*^{spin} (KO × KO; hereafter DKO mice). However, DKO mice were not born at the expected Mendelian ratio. Of the expected 12.5% DKO mice from our breeding strategy, only 6.5% DKO mice were born, i.e., a 50% reduction in the expected birth of the DKO mice (Fig. 1A). We have seen similar deficiencies in the birth of DKO mice from other breeder pairs as well. Moreover, the DKO mice that were born were smaller in size when compared to their littermate controls (Fig. 1B). About 50 to 60% of these DKO mice died spontaneously following birth (Fig. 1C), demonstrating an important role for CD47 in the survival of the *Ptpn6*^{spin} mice. Following the surviving DKO mice longitudinally, we observed that most of these mice also developed footpad swelling, although severity was similar between DKO and *Ptpn6*^{spin} littermate controls (Fig. 1D). These data together demonstrate a previously unknown protective role for CD47 in the survival of *Ptpn6*^{spin} mice.

Radioresistant CD47 is required for survival of *Ptpn6*^{spin} mice

We have previously shown that spontaneous inflammatory disease in *Ptpn6*^{spin} mice is driven by myeloid cells (*9*, *12*). *Ptpn6*^{spin} bone marrow cells, when transferred into lethally irradiated wild-type (WT) mice (*Ptpn6*^{spin} >> WT chimeras), develop footpad inflammation, but importantly, none of these chimera mice die. We next investigated the consequence of *Ptpn6*^{spin} bone marrow cells transferred into lethally irradiated *Cd47*-deficeint mice (*Ptpn6*^{spin} >> *Cd47*$^{-/-}$ chimeras). *Ptpn6*^{spin} >> *Cd47*$^{-/-}$ chimeras began to die around day 30 after chimerism, and all mice were dead by day 60 (fig. S2). *Ptpn6*^{spin} cells promoted the death of *Cd47*$^{-/-}$ recipients because WT >> *Cd47*$^{-/-}$ chimeras were normal and healthy (fig. S2). To examine the cause of death of *Ptpn6*^{spin} >> *Cd47*$^{-/-}$ chimeras, we monitored their weight loss following the induction of chimera. In contrast to healthy WT >> *Cd47*$^{-/-}$ chimeras, *Ptpn6*^{spin} >> *Cd47*$^{-/-}$ chimera mice gradually lost weight and never recovered, with as much as 60% of chimera mice dying by the end of the experiment (Fig. 2, A and B). The difference in health status was evident by the marked difference in size of the runted *Ptpn6*^{spin} >> *Cd47*$^{-/-}$ chimera mice when compared to WT >> *Cd47*$^{-/-}$ chimeras (Fig. 2C). Furthermore, the footpad inflammation was also evident in the *Ptpn6*^{spin} >> *Cd47*$^{-/-}$ chimera (Fig. 2D). Analysis of the *Ptpn6*^{spin} >> *Cd47*$^{-/-}$ chimera spleens revealed that the spleens were markedly reduced in size, and histological analysis showed lack of lymphoid follicles (Fig. 2E). As could be expected, splenic weight and splenocyte numbers were markedly reduced in the *Ptpn6*^{spin} >> *Cd47*$^{-/-}$ mice when compared to WT >> *Cd47*$^{-/-}$ chimeras (Fig. 2F). The morbidity and mortality observed in *Ptpn6*$^{spin/spin}$ >> *Cd47*$^{-/-}$ chimeras was not observed in *Ptpn6*$^{spin/+}$ >> *Cd47*$^{-/-}$ chimeras, which suggests that the heterozygosity of spin mutation in the bone marrow compartment is not sufficient to drive lethal disease in *Cd47*$^{-/-}$ mice (fig. S3, A to C). *Ptpn6*$^{spin/+}$ and *Ptpn6*$^{spin/spin}$ mice used in these experiments were littermates, which excludes a potential effect of microbiota in the *Ptpn6* background. In concurrence with the disease outcome, spleen size and cellularity were significantly reduced in *Ptpn6*$^{spin/spin}$ >> *Cd47*$^{-/-}$ chimeras when compared to disease-free *Ptpn6*$^{spin/+}$ >> *Cd47*$^{-/-}$ chimeras (fig. S3D).

Splenic cellular analysis of *Ptpn6*^{spin} >> *Cd47*$^{-/-}$ chimeras exhibits marked changes in lymphoid and myeloid populations

Lymphoid organs, including the spleen, are dominated by adaptive cells that include T and B cells (*31*). As observed in hematoxylin and eosin (H&E) stains, normal lymphoid follicles observed in WT >> *Cd47*$^{-/-}$ spleen are absent in *Ptpn6*^{spin} >> *Cd47*$^{-/-}$ spleen (Fig. 2E). Flow cytometric analysis of the splenocytes for various populations showed that CD4^{+} and CD8^{+} T cell populations were significantly reduced (Fig. 3A). While CD19^{+}MHCII^{+} (major histocompatibility complex II positive) B cell frequency was significantly reduced in *Ptpn6*^{spin} >> *Cd47*$^{-/-}$ mice, MHCII expression in these B cells from *Ptpn6*^{spin} >> *Cd47*$^{-/-}$ spleens was significantly increased, suggesting increased activation (Fig. 3, B and C). In contrast to lymphoid cells, the frequency of CD11b^{+}Ly6G^{+} neutrophil and CD11b^{+}Ly6G^{-} monocyte populations was significantly increased in the spleens of *Ptpn6*^{spin} >> *Cd47*$^{-/-}$ chimeras when compared to WT >> *Cd47*$^{-/-}$ chimeras (Fig. 3D). Similar reductions in lymphoid cell populations and increases in myeloid cell populations were also observed in *Ptpn6*$^{spin/spin}$ >> *Cd47*$^{-/-}$ chimeras when compared to *Ptpn6*$^{spin/+}$ >> *Cd47*$^{-/-}$ chimeras (fig. S3, E to H). Together, these data suggest that *Ptpn6*^{spin} cells, when transferred to *Cd47*-deficient recipients, result in lymphopenia and neutrophilia. To examine whether *Ptpn6*^{spin} cells alone are sufficient to induce this dysregulation in immune cell populations, we compared immune populations of *Ptpn6*^{spin} >> *Cd47*$^{-/-}$ chimeras with *Ptpn6*^{spin} >> WT chimeras (fig. S4, A to E). Both T and B cell populations were observed at normal frequency in *Ptpn6*^{spin} >> WT mouse spleens. Compared to *Ptpn6*^{spin} >> WT, *Ptpn6*^{spin} >> *Cd47*$^{-/-}$ chimeras had significantly reduced lymphoid cells and increased myeloid cells (fig. S4, A to E). Thus, *Ptpn6*^{spin} cells are not sufficient to drive the observed dysregulation of immune cell populations in *Ptpn6*^{spin} >> *Cd47*$^{-/-}$ chimeras.

A

Breeders:
Male: *CD47*$^{+/-}$ x *Ptpn6*$^{spin/spin}$ (HK)
Female: *CD47*$^{+/-}$ x *Ptpn6*$^{spin/+}$ (HH)

Genotype	Observed offspring	Expected frequency	Observed frequency
WT × HT	13/61	12.5	21.31
WT × KO	8/61	12.5	13.11
HT × HT	13/61	25	21.31
HT × KO	14/61	25	22.95
KO × HT	9/61	12.5	14.75
KO × KO	4/61	12.5	6.56
Total	61/61	100	99.99

B

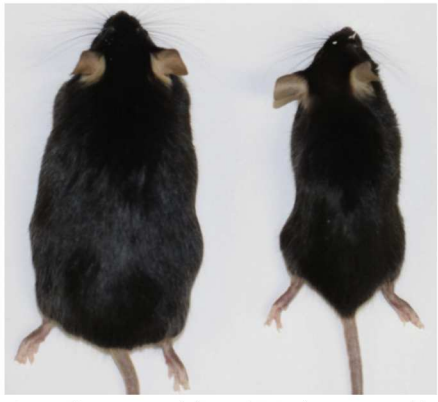

CD47$^{+/+}$ x *Ptpn6*$^{spin/+}$ (WT × HT)
CD47$^{-/-}$ x *Ptpn6*$^{spin/spin}$ (DKO)

C

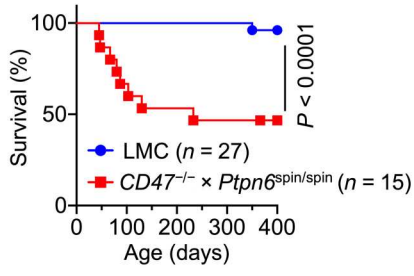

D

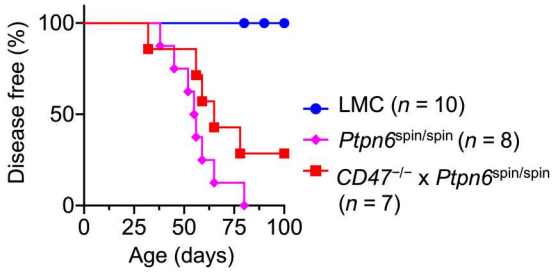

Fig. 1. *Cd47*$^{-/-}$ × *Ptpn6*$^{spin/spin}$ DKO mice are not born at an expected Mendelian ratio. (**A**) *Cd47*$^{+/-}$ × *Ptpn6*$^{spin/spin}$ (HK) male mice were bred with *CD47*$^{+/-}$ × *Ptpn6*$^{spin/+}$ (HH) female mice to generate *Ptpn6*^{spin} mice deficient in *CD47*, i.e., *Cd47*$^{-/-}$ × *Ptpn6*^{spin} double-knockout (DKO) mice. (**B**) Images of *CD47*$^{-/-}$ × *Ptpn6*$^{spin/spin}$ (DKO) mouse compared to littermate control (*Cd47*$^{+/+}$ × *Ptpn6*$^{spin/+}$). (**C**) Survival of *Cd47*$^{-/-}$ × *Ptpn6*^{spin} (DKO) mice over time compared to littermate controls (LMC; includes all other genotypes). (**D**) Incidence of spontaneous footpad inflammation in *CD47*$^{-/-}$ × *Ptpn6*^{spin} DKO mice compared to *Ptpn6*^{spin} mice and littermate controls (LMC; excludes *Ptpn6*^{spin} mice) that survived more than 3 months.

Ptpn6-deficient neutrophils drive morbidity and mortality in *Cd47*-deficient recipients

Our data to date have shown that *Ptpn6*^{spin} hematopoietic cells provoke morbidity and mortality when transferred into a *Cd47*-deficient recipient. We have previously shown that *Ptpn6* deficiency in the myeloid compartment (*Ptpn6*$^{fl/fl}$ × *Lyz2*-Cre mice; hereafter *Ptpn6*$^{\Delta myeloid}$ mice) is sufficient to mimic the spontaneous footpad inflammation observed in the *Ptpn6*^{spin} mice (*12*). Therefore, we tested whether *Ptpn6*$^{\Delta myeloid}$ cells were sufficient to provoke lethal disease in *Cd47*-deficient mice. To this end, we transferred *Ptpn6*$^{\Delta myeloid}$ bone marrow cells into lethally irradiated *Cd47*$^{-/-}$ mice to generate *Ptpn6*$^{\Delta myeloid}$ >> *Cd47*$^{-/-}$ chimeras. Similar to the *Ptpn6*^{spin} >> *Cd47*$^{-/-}$ chimeras, all *Ptpn6*$^{\Delta myeloid}$ >> *Cd47*$^{-/-}$ chimeras were dead by day 60 after chimerism (Fig. 4A). *Ptpn6*$^{\Delta myeloid}$ cells alone are not sufficient to cause this lethality, as *Ptpn6*$^{\Delta myeloid}$ >> WT mice do not die following chimerism and survive up to 120 days after chimerism (fig. S4F). *Ptpn6*$^{\Delta myeloid}$ >> *Cd47*$^{-/-}$ mice progressively lost more weight compared to WT >> *Cd47*$^{-/-}$ mice following chimera generation (Fig. 4B). These *Ptpn6*$^{\Delta myeloid}$ >> *Cd47*$^{-/-}$ chimera mice appeared significantly smaller than WT >> *Cd47*$^{-/-}$ chimeras and presented with inflamed footpads and smaller spleens at study end (~60 days; Fig. 4, C and D). Furthermore, T and B cell populations were reduced, while neutrophil and monocyte populations were significantly increased in *Ptpn6*$^{\Delta myeloid}$ >> *Cd47*$^{-/-}$ chimera spleens when compared to those of WT >> *Cd47*$^{-/-}$ chimera mice (Fig. 4, E to H). These results suggest that deletion of *Ptpn6* in myeloid cells in *Ptpn6*$^{\Delta myeloid}$ mice, which include neutrophils, monocytes, and macrophages, provokes lethal inflammation in *Cd47*-deficient mice (*32*).

Within the myeloid compartment, it is believed that neutrophils are the primary cells that provoke autoinflammatory disease in *Ptpn6*^{spin} mice (*7*). Mice with *Ptpn6* deletion, specifically in the neutrophil population (*Ptpn6*$^{fl/fl}$ × *S100a8*-Cre mice; hereafter *Ptpn6*$^{\Delta PMN}$ mice), develop spontaneous footpad inflammation similar to that observed in *Ptpn6*^{spin} mice (*10*, *33*). We have also generated *Ptpn6*$^{\Delta PMN}$ mice in our laboratory and find that these mice develop spontaneous footpad inflammation with 100% penetrance at about 6 to 16 weeks of age (fig. S5A). Thus, we posited that *Ptpn6*-deficienct neutrophils provoke fatal disease in *Cd47*$^{-/-}$ mice. To this end, we generated *Ptpn6*$^{\Delta PMN}$ >> *Cd47*$^{-/-}$ chimera mice and followed them for morbidity and mortality. While WT >> *Cd47*$^{-/-}$ chimeras recovered as expected, *Ptpn6*$^{\Delta PMN}$ >> *Cd47*$^{-/-}$ chimeras began dying at around 2 weeks, with 100% dying by day 60 after chimerism (Fig. 5A). The observed lethality in *Ptpn6*$^{\Delta PMN}$ >> *Cd47*$^{-/-}$ chimeras requires both SHP1 and

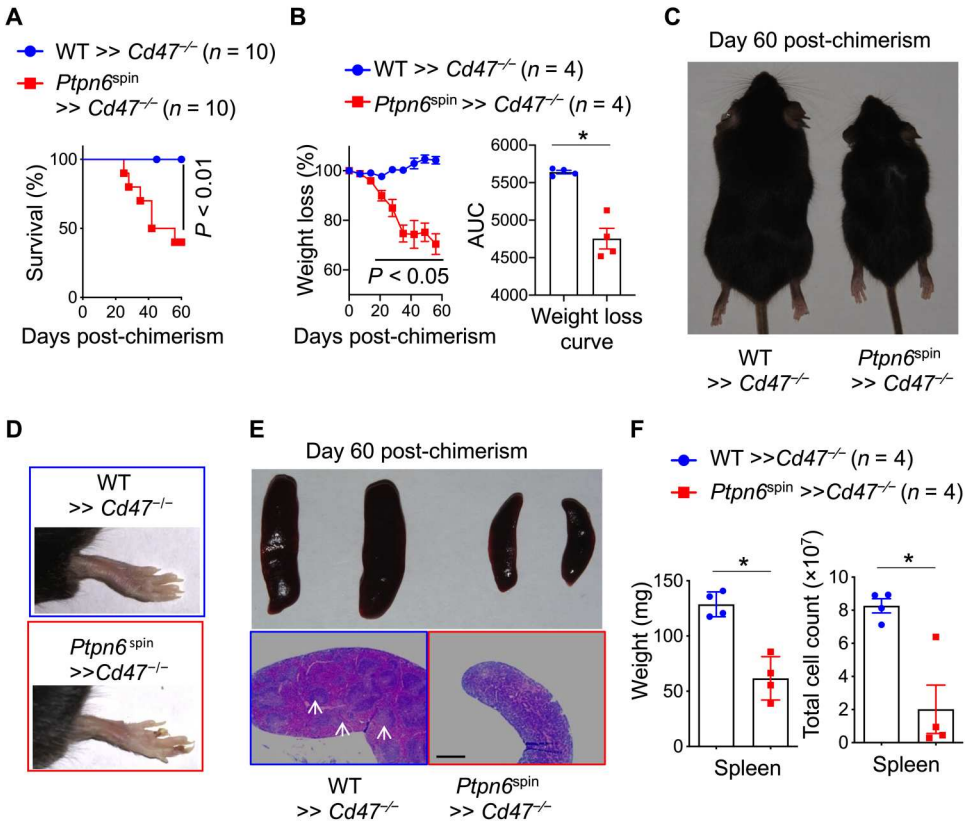

Fig. 2. *Ptpn6*^{spin} bone marrow cells are sufficient to cause wasting of lethally irradiated *Cd47*-deficient recipient mice. To examine the role of CD47 in the radioresistant compartment, bone marrow chimera was generated by transferring C57BL/6 WT or *Ptpn6*^{spin} bone marrow cells into *Cd47*$^{-/-}$ mice, i.e., WT >> *Cd47*$^{-/-}$ versus *Ptpn6*^{spin} >> *Cd47*$^{-/-}$ chimera mice. (**A**) Percent survival of WT >> *Cd47*$^{-/-}$ (*N* = 10) versus *Ptpn6*^{spin} >> *Cd47*$^{-/-}$ (*N* = 10) chimera mice. (**B**) Percent weight loss of WT >> *Cd47*$^{-/-}$ (*N* = 4) versus *Ptpn6*^{spin} >> *Cd47*$^{-/-}$ (*N* = 4) chimera mice (left) and area under the curve (AUC) of weight loss for each individual mouse (right). (**C**) Representative image of WT >> *Cd47*$^{-/-}$ and *Ptpn6*^{spin} >> *Cd47*$^{-/-}$ chimera mice on day 60 after chimerism. (**D**) Representative image of diseased footpad from *Ptpn6*^{spin} >> *Cd47*$^{-/-}$ chimera mice compared to WT >> *Cd47*$^{-/-}$ chimera mice. (**E**) Representative images of spleens (top) and hematoxylin and eosin (H&E) stain (bottom) from WT >> *Cd47*$^{-/-}$ and *Ptpn6*^{spin} >> *Cd47*$^{-/-}$ chimera mice on day 60 after chimerism; arrowheads show lymphoid follicles present in WT >> *Cd47*$^{-/-}$ spleens, which are completely abrogated in *Ptpn6*^{spin} >> *Cd47*$^{-/-}$ chimera mice. H&E image: ×4 magnification. Scale bar, 0.5 mm. (**F**) Splenic weight (left) and total splenocyte count (right) from WT >> *Cd47*$^{-/-}$ and *Ptpn6*^{spin} >> *Cd47*$^{-/-}$ chimera mice on day 60 after chimerism. Data are representative of at least two independent experiments. All data are presented as means ± SEM. Survival curves were analyzed using the log-rank (Mantel-Cox) test. Statistical significance between two groups was determined using Mann-Whitney *t* tests. *P* values less than 0.05 were considered statistically significant. *$P \leq 0.05$.

CD47 deficiency, because *Ptpn6*$^{\Delta PMN}$ >> WT mice do not show any signs of systemic disease and survive the length of the study (fig. S5B). *Ptpn6*$^{\Delta PMN}$ >> *Cd47*$^{-/-}$ chimeras showed obvious signs of disease as demonstrated by weight loss, runting, and inflamed footpads (Fig. 5B and fig. S5C). Specifically, these mice developed substantial footpad lesions and tail pathology, which required us to humanely end the experiment to reduce unnecessary suffering. *Ptpn6*$^{\Delta PMN}$ >> *Cd47*$^{-/-}$ chimeras also had smaller spleens when compared to WT >> *Cd47*$^{-/-}$ chimera mice (Fig. 5, B and C). Flow cytometry analysis of splenocytes showed that CD4$^+$, CD8$^+$, and CD19$^+$ lymphoid cells were significantly reduced in *Ptpn6*$^{\Delta PMN}$ >> *Cd47*$^{-/-}$ chimeras (Fig. 5, D to F). CD19$^+$MHCII$^+$ splenic B cells from *Ptpn6*$^{\Delta PMN}$ >> *Cd47*$^{-/-}$ chimeras did not have higher levels of MHCII expression when compared to WT >> *Cd47*$^{-/-}$ chimeras (Fig. 5G). Both neutrophil and monocyte populations were significantly increased in *Ptpn6*$^{\Delta PMN}$ >> *Cd47*$^{-/-}$ chimera spleens (Fig. 5H). In summary, these data show that *Ptpn6* neutrophil deficiency is sufficient to drive fatal disease in *Cd47*-deficient mice. To further investigate whether *Ptpn6*$^{\Delta PMN}$ cells alone are sufficient to promote immune cell dysregulation, we compared immune populations of *Ptpn6*$^{\Delta PMN}$ >> *Cd47*$^{-/-}$ chimeras with *Ptpn6*$^{\Delta PMN}$ >> WT chimeras (fig. S6). Compared to *Ptpn6*$^{\Delta PMN}$ >> WT, *Ptpn6*$^{\Delta PMN}$ >> *Cd47*$^{-/-}$ chimeras had significantly reduced lymphoid cells and increased myeloid cells (fig. S6). Thus, *Ptpn6*$^{\Delta PMN}$ cells alone cannot drive the immune cell dysregulation in *Ptpn6*$^{\Delta PMN}$ >> *Cd47*$^{-/-}$ chimeras.

Ptpn6^{spin} bone marrow cells demonstrate a dominant effect over WT bone marrow cells when transferred into CD47-deficient recipients

Given the morbidity and mortality of *Ptpn6*^{spin} >> *Cd47*$^{-/-}$ chimeras, it could be argued that *Ptpn6*^{spin} bone marrow cells fail to reconstitute lethally irradiated *Cd47*$^{-/-}$ mice, which would explain the morbidity and mortality observed in these chimeras. To address this, congenically marked CD45.1 *Ptpn6*^{spin} bone marrow cells were mixed with CD45.2 WT C57BL/6 bone marrow cells at a 1:1 ratio and adoptively transferred into lethally irradiated *Cd47*$^{-/-}$ mice (Fig. 6A). While all lethally irradiated *Cd47*$^{-/-}$

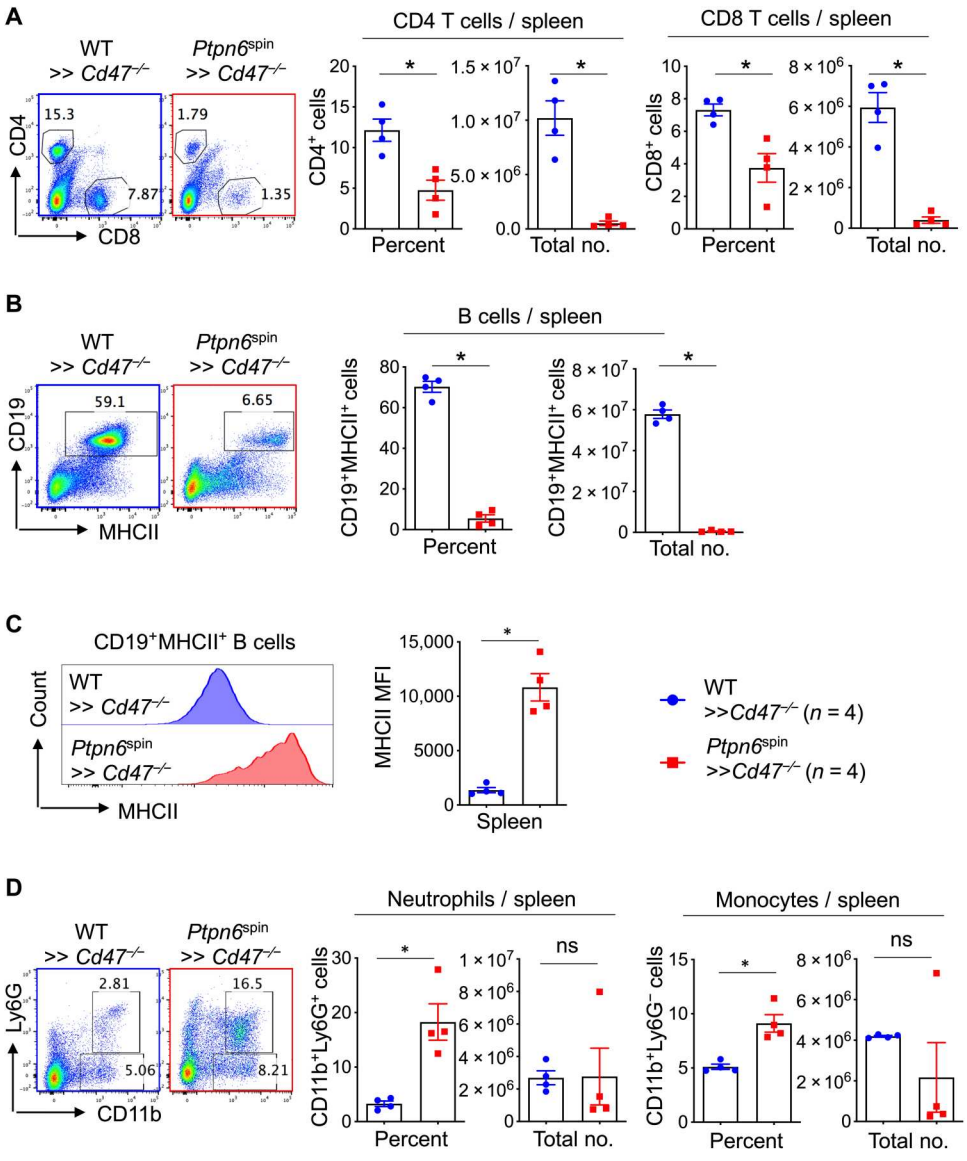

Fig. 3. Analysis of *Ptpn6*^{spin} >> *Cd47*$^{-/-}$ chimera splenic immune cells shows significantly reduced lymphoid and increased myeloid cells when compared to WT >> *Cd47*$^{-/-}$ chimeras. Flow cytometric analysis of splenocytes from WT >> *Cd47*$^{-/-}$ and *Ptpn6*^{spin} >> *Cd47*$^{-/-}$ chimeras on day 60 after chimerism. (**A**) Representative flow plot (left) and cumulative data shown as percentage and total cell numbers (right) for CD4$^+$ T cells and CD8$^+$ T cells. (**B**) Representative flow plot (left) and cumulative data shown as percentage and total cell numbers (right) for CD19$^+$MHCII$^+$ B cells. (**C**) Representative offset histogram plots (left) and cumulative data (right) depicting MHCII mean expression levels on CD19$^+$MHCII$^+$ B cells. (**D**) Representative flow plot (left) and cumulative data shown as percentage and total cell numbers (right) for CD11b$^+$Ly6G$^+$ neutrophil and CD11b$^+$Ly6G$^-$ monocyte populations. These data are representative of at least two independent experiments, and each dot represents an individual mouse. Statistical significance between two groups was determined using Mann-Whitney *t* tests. Data are means ± SEM. *P* values less than 0.05 were considered statistically significant. *$P \leq 0.05$.

mice receiving 1:1 mix of WT (45.1) + WT (45.2) bone marrow cells survived, *Cd47*$^{-/-}$ mice receiving 1:1 mix of WT (45.1) + *Ptpn6*^{spin} (45.2) bone marrow cells started to die, with around 60% dying by day 40, at which point the remaining mice were harvested (Fig. 6B). Like the *Ptpn6*^{spin} >> *Cd47*$^{-/-}$ chimeras, WT (45.1) + *Ptpn6*^{spin} (45.2) >> *Cd47*$^{-/-}$ chimeras also lost significantly more weight when compared to WT (45.1) + WT (45.2) >> *Cd47*$^{-/-}$ chimeras (Fig. 6C). These data argue against the idea that *Ptpn6*^{spin} bone marrow cells fail to reconstitute the *Cd47*$^{-/-}$ mice and further suggest that *Ptpn6*^{spin} cells dominantly promote morbidity and mortality in *Cd47*$^{-/-}$ recipients. Given that the WT (45.1) + *Ptpn6*^{spin} (45.2) >> *Cd47*$^{-/-}$ chimeras had equal proportions of WT (45.1) and *Ptpn6*^{spin} (45.2) donor bone marrow cells, we sought to determine whether the proportion of these cells had changed in the diseased chimeras. Compared to WT (45.1) + WT (45.2) >> *Cd47*$^{-/-}$ chimeras, splenocyte counts were significantly reduced in the diseased WT (45.1) + *Ptpn6*^{spin} (45.2) >> *Cd47*$^{-/-}$ chimeras (Fig. 6D). When we analyzed the frequency of CD45.1 versus CD45.2 cells in the spleen within each chimera, the ratio of CD45.1 versus CD45.2 cells in both healthy WT (45.1) + WT (45.2)

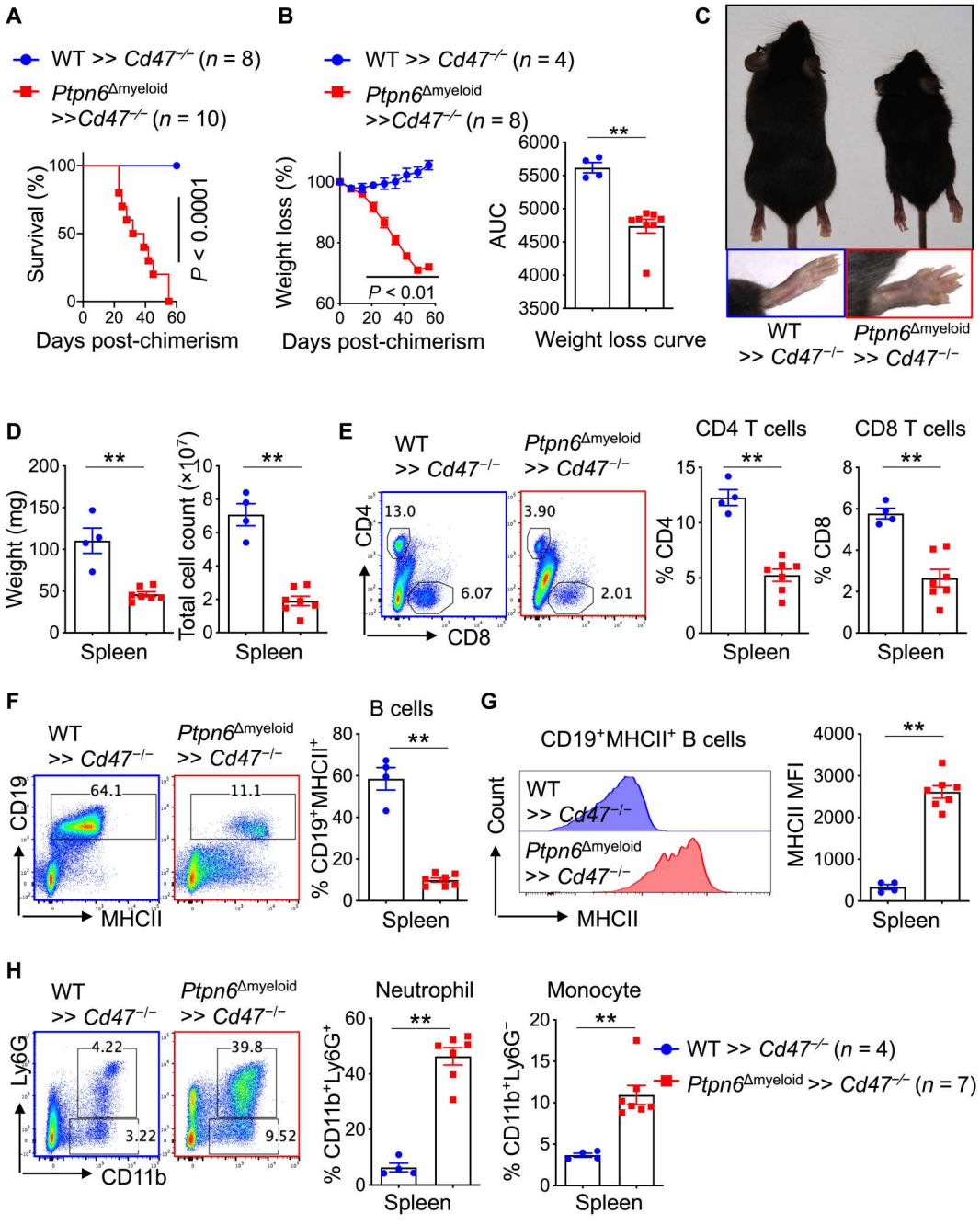

Fig. 4. *Ptpn6*-deficient myeloid cells promote morbidity and mortality of *Cd47*$^{-/-}$ mice following chimerism. *Ptpn6*$^{fl/fl}$ mice were bred with *Lyz2*-Cre mice to generate mice with myeloid-specific deletion of *Ptpn6* (*Ptpn6*$^{\Delta myeloid}$). Chimera mice were generated by transferring WT or *Ptpn6*$^{\Delta myeloid}$ bone marrow cells into lethally irradiated *Cd47*$^{-/-}$ mice, i.e., WT >> *Cd47*$^{-/-}$ and *Ptpn6*$^{\Delta myeloid}$ >> *Cd47*$^{-/-}$ chimera mice. (**A**) Percent survival of WT >> *Cd47*$^{-/-}$ (N = 8) versus *Ptpn6*$^{\Delta myeloid}$ >> *Cd47*$^{-/-}$ (N = 10) chimera mice. (**B**) Weight loss in WT >> *Cd47*$^{-/-}$ and *Ptpn6*$^{\Delta myeloid}$ >> *Cd47*$^{-/-}$ mice following chimerism presented as percent weight loss (left) and AUC of weight loss for each individual mouse (right). (**C**) Representative image of WT >> *Cd47*$^{-/-}$ and *Ptpn6*$^{\Delta myeloid}$ >> *Cd47*$^{-/-}$ chimera mice (top) and representative image of their footpads (bottom) on day 60 after chimerism. (**D**) Spleen weight (left) and total splenocyte count (right) from *Ptpn6*$^{\Delta myeloid}$ >> *Cd47*$^{-/-}$ chimeras compared to WT >> *Cd47*$^{-/-}$ chimeras. (**E** to **H**) Flow cytometric analysis of splenocytes from WT >> *Cd47*$^{-/-}$ and *Ptpn6*$^{\Delta myeloid}$ >> *Cd47*$^{-/-}$ chimera mice on day 60 after chimerism. (E) Representative flow plot (left) and cumulative data (right) for CD4$^+$ T cells and CD8$^+$ T cells. (F) Representative flow plot (left) and cumulative data (right) for CD19^{+-} MHCII$^+$ B cells. (G) Representative offset histogram plots (left) and cumulative data (right) depicting MHCII mean expression levels on CD19$^+$MHCII$^+$ B cells. (H) Representative flow plot (left) and cumulative data (right) for CD11b$^+$Ly6G$^+$ neutrophil and CD11b$^+$Ly6G$^-$ monocyte populations. Each dot represents an individual mouse. Statistical significance was determined using Mann-Whitney t tests. Data are means ± SEM. P values less than 0.05 were considered statistically significant. **$P \leq 0.01$.

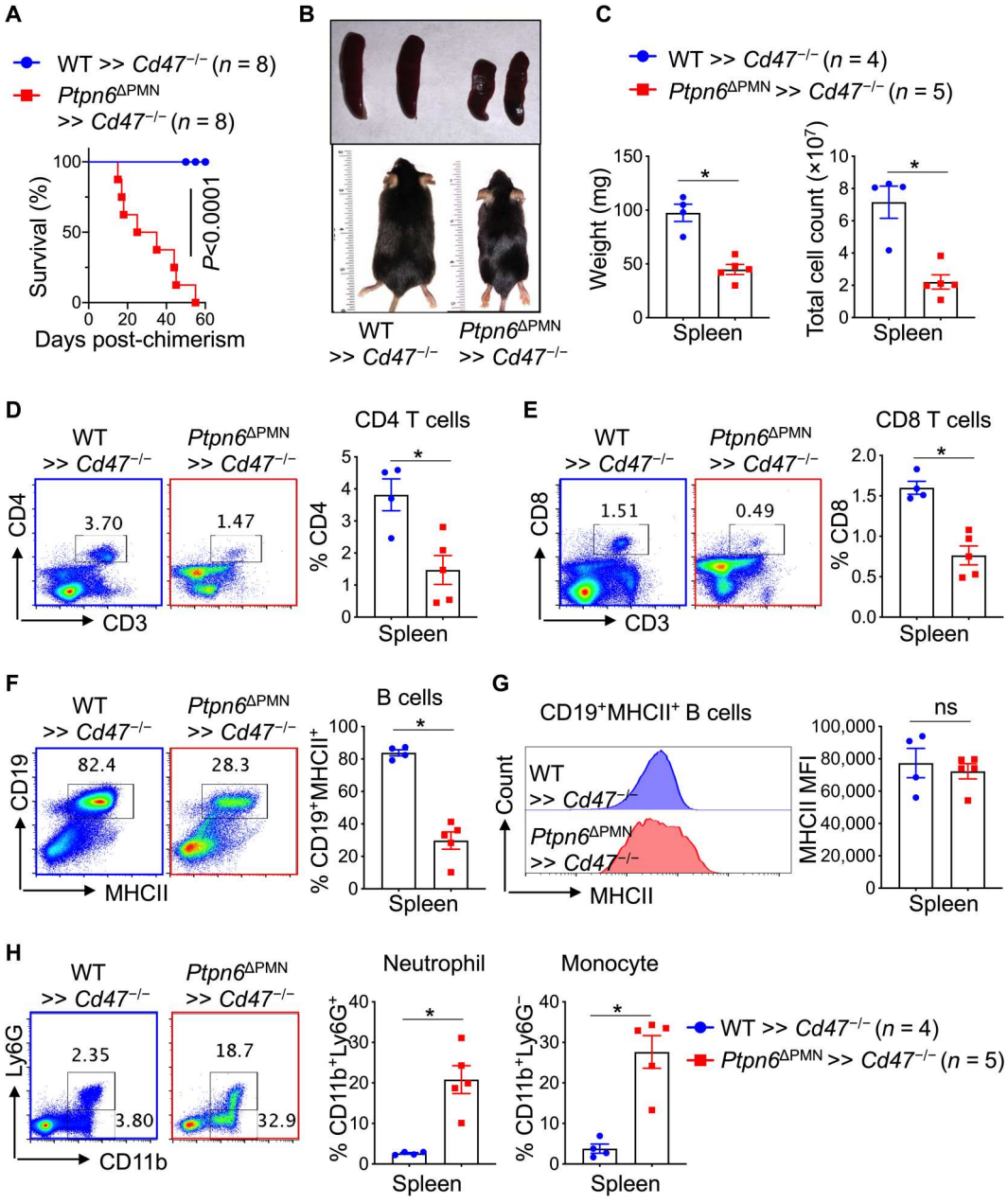

Fig. 5. *Ptpn6*-deficient neutrophils drive morbidity and mortality in *Cd47*-deficient recipients. *Ptpn6*$^{fl/fl}$ mice were bred with *S100a8*-Cre mice to generate mice with neutrophil-specific deficiency of *Ptpn6* (*Ptpn6*$^{\Delta PMN}$) mice. WT >> *Cd47*$^{-/-}$ and *Ptpn6*$^{\Delta PMN}$ >> *Cd47*$^{-/-}$ bone marrow chimera mice were generated by transferring WT and *Ptpn6*$^{\Delta PMN}$ bone marrow cells into lethally irradiated *Cd47*$^{-/-}$ mice. (**A**) Percent survival of WT >> *Cd47*$^{-/-}$ ($N = 8$) versus *Ptpn6*$^{\Delta PMN}$ >> *Cd47*$^{-/-}$ ($N = 8$) chimera mice. (**B**) Representative image of WT >> *Cd47*$^{-/-}$ and *Ptpn6*$^{\Delta PMN}$ >> *Cd47*$^{-/-}$ chimera mice (B, bottom) and spleen (B, top). (**C**) Splenic weight (left) and number (right) on day 34 after chimerism. (**D** to **H**) Flow cytometric analysis of the splenocytes from WT >> *Cd47*$^{-/-}$ and *Ptpn6*$^{\Delta PMN}$ >> *Cd47*$^{-/-}$ chimera mice on day 34 after chimerism. (D) Representative flow plot (left) and cumulative data (right) for CD3$^+$CD4$^+$ T cells. (E) Representative flow plot (left) and cumulative data (right) for CD3$^+$CD8$^+$ T cells. (F) Representative flow plot (left) and cumulative data (right) for CD19$^+$MHCII$^+$ B cells. (G) Representative offset histogram plots (left) and cumulative data (right) depicting MHCII mean expression levels on CD19$^+$MHCII$^+$ B cells. (H) Representative flow plot (left) and cumulative data (right) for CD11b$^+$Ly6G$^+$ neutrophil and CD11b$^+$Ly6G$^-$ monocyte populations. Each dot represents an individual mouse. Statistical significance was determined using Mann-Whitney *t* tests. Data are means ± SEM. *P* values less than 0.05 were considered statistically significant. *$P \leq 0.05$. ns, not significant.

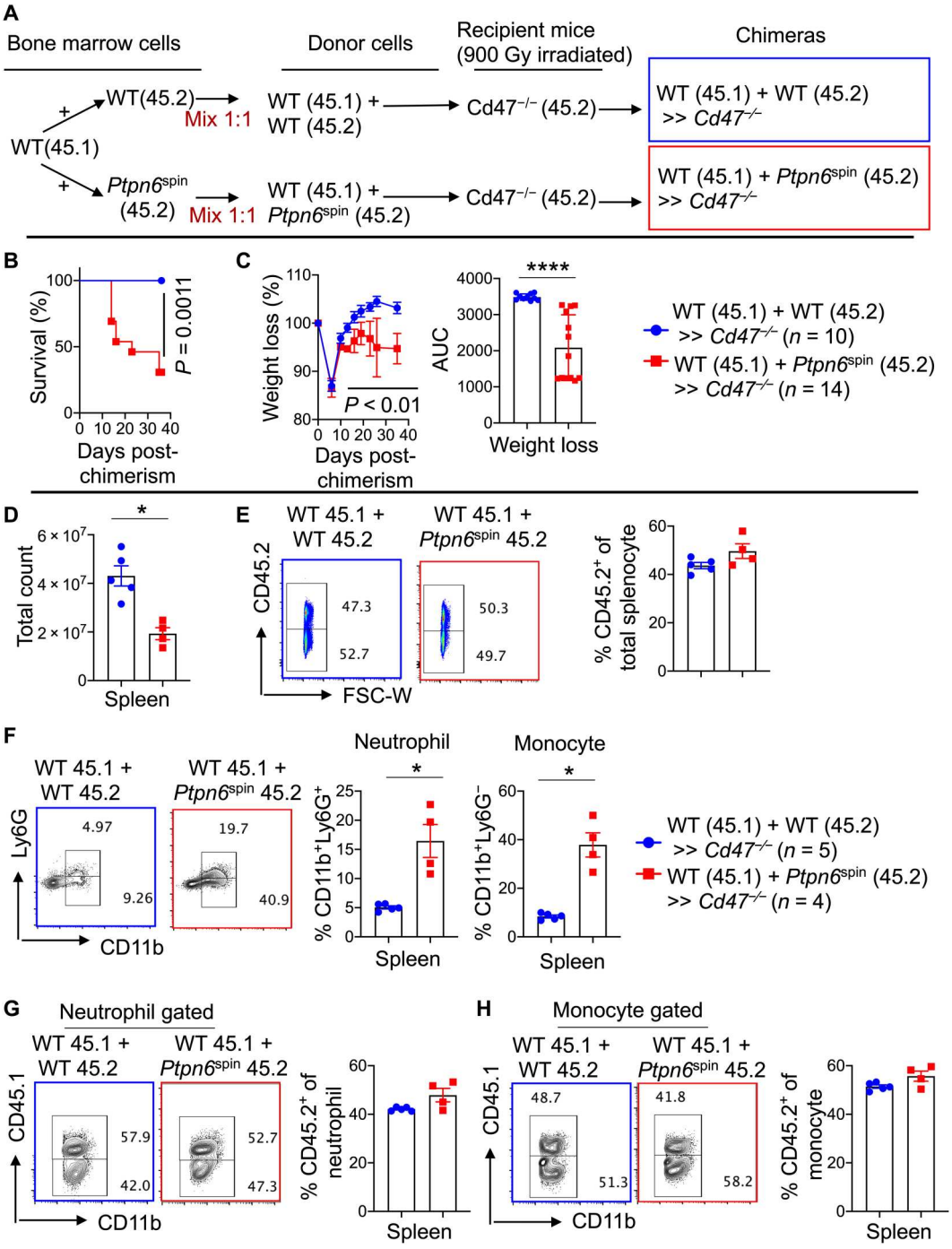

Fig. 6. Mixed bone marrow chimera with 1:1 transfer of *Ptpn6*^{spin} and WT into *Cd47*$^{-/-}$ mice demonstrates dominant role of *Ptpn6*^{spin} immune cells in promoting morbidity and mortality. (**A**) Experimental design to examine the role of *Ptpn6*^{spin} bone marrow cells in a competitive chimera. Briefly, CD45.1 C57BL/6 were mixed with CD45.2 C57BL/6 or CD45.2 *Ptpn6*^{spin} bone marrow cells at 1:1 ratio to generate CD45.1 WT + CD45.2 WT or CD45.1 WT + CD45.2 *Ptpn6*^{spin} donor cells. These donor cells were then transferred into lethally irradiated (9 Gy) *Cd47*$^{-/-}$ mice to generate respective chimeras. (**B**) Survival of WT (45.1) + WT (45.2) >> *Cd47*$^{-/-}$ versus WT (45.1) + *Ptpn6*^{spin} (45.2) >> *Cd47*$^{-/-}$ mice. (**C**) Percent weight loss (left) and AUC of weight loss for individual mice for WT (45.1) + WT (45.2) >> *Cd47*$^{-/-}$ versus WT (45.1) + *Ptpn6*^{spin} (45.2) >> *Cd47*$^{-/-}$ mice. (**D**) Total splenocyte count in WT (45.1) + WT (45.2) >> *Cd47*$^{-/-}$ and WT (45.1) + *Ptpn6*^{spin} (45.2) >> *Cd47*$^{-/-}$ mice. (**E** to **H**) Flow cytometric analysis of splenocytes from WT (45.1) + WT (45.2) >> *Cd47*$^{-/-}$ and WT (45.1) + *Ptpn6*^{spin} (45.2) >> *Cd47*$^{-/-}$ chimeras. (E) Representative flow plot demonstrating frequency of CD45.2$^+$ cells (left) and cumulative data (right) in splenocytes. (F) Representative flow plot demonstrating CD11b$^+$Ly6G$^+$ neutrophil and CD11b$^+$Ly6G$^-$ monocyte populations (left) and cumulative data (right) in splenocyte population. (G) Representative flow plot demonstrating CD45.2$^+$ neutrophil population based on CD45.1 stain (left) and cumulative data (right). (H) Representative flow plot demonstrating CD45.2$^+$ monocyte population based on CD45.1 stain (left) and cumulative data (right). Each dot represents an individual mouse. Statistical significance was determined using Mann-Whitney *t* tests. Data are means ± SEM. *P* values less than 0.05 were considered statistically significant. *$P \leq 0.05$ and ****$P \leq 0.0001$.

>> *Cd47*$^{-/-}$ and diseased WT (45.1) + *Ptpn6*^{spin} (45.2) >> *Cd47*$^{-/-}$ chimeras was 1:1 (Fig. 6E). As observed previously, the frequency of neutrophils and monocytes in diseased WT (45.1) + *Ptpn6*^{spin} (45.2) >> *Cd47*$^{-/-}$ chimera spleens was significantly increased (Fig. 6F). The proportion of WT (45.1) versus *Ptpn6*^{spin} (45.2) cells within the neutrophil and monocyte populations was a 1:1 ratio (Fig. 6, G and H). These data demonstrate that the dominant effect of *Ptpn6*^{spin} bone marrow cells to provoke morbidity and mortality in *Cd47*$^{-/-}$ recipients is not due to their ability to outcompete WT bone marrow cells. Further analysis of T cells, B cells, and natural killer (NK) cell populations recapitulated previous observations with reduced overall frequency of T cells and B cells in diseased chimeras (fig. S7). While the proportion of WT (45.1) versus *Ptpn6*^{spin} (45.2) cells within the CD4$^+$ and CD8$^+$ T cells was a 1:1 ratio, the proportion of *Ptpn6*^{spin} (45.2) cells within the B cell and NK cell compartments was significantly reduced, with WT (45.2) cells dominating the proportion (fig. S7, E and F). These data together demonstrate that *Ptpn6*^{spin} cells are dominant over WT bone marrow cells in their ability to promote morbidity and mortality when transferred at an equal ratio in lethally irradiated *Cd47*$^{-/-}$ recipients.

Ptpn6^{spin} cells promote colonic cell death and gut leakage in *Cd47*-deficient mice

To identify the mechanisms that promote morbidity and mortality in *Ptpn6*^{spin} >> *Cd47*$^{-/-}$ chimeras, whole-body necropsies were performed. As expected, WT >> *Cd47*$^{-/-}$ mice were mostly without notable lesion. However, *Ptpn6*^{spin} >> *Cd47*$^{-/-}$ mice showed inflammation and disease in multiple organs, including spleen, lymph node, heart, lungs, liver, bone, colon, and cecum (fig. S8). Specifically, ceca and colons from *Ptpn6*^{spin} >> *Cd47*$^{-/-}$ mice looked markedly different when compared to WT >> *Cd47*$^{-/-}$ mice. Ceca from *Ptpn6*^{spin} >> *Cd47*$^{-/-}$ mice were devoid of fecal matter and coiled around in the colon (Fig. 7A). Given cecum and colon presentation, we posited that gut leakage may contribute to the observed morbidity and mortality of *Ptpn6*^{spin} >> *Cd47*$^{-/-}$ mice. In concordance, spleen lysates from *Ptpn6*^{spin} >> *Cd47*$^{-/-}$ but not WT >> *Cd47*$^{-/-}$ mice grew positive bacterial colonies when plated on tryptic soy broth (TSB) agar plates (Fig. 7B). Eight of 11 *Ptpn6*^{spin} >> *Cd47*$^{-/-}$ spleens had positive bacterial colonies, while all 8 WT >> *Cd47*$^{-/-}$ spleens were negative (Fig. 7B). Histological analysis of colon tissues showed that *Ptpn6*^{spin} >> *Cd47*$^{-/-}$ mice had higher levels of inflammation characterized by neutrophilic infiltration, crypt micro-abscesses, and loss of goblet cells (Fig. 7C). Tissue scoring (see Materials and Methods) of colonic H&E sections showed that *Ptpn6*^{spin} >> *Cd47*$^{-/-}$ mice had significantly higher inflammatory scores compared to WT >> *Cd47*$^{-/-}$ mice (Fig. 7D).

Given these findings, we hypothesized that *Ptpn6*^{spin} cells promote excessive cell death and gut leakage in *Cd47*$^{-/-}$ mice during chimerism. To examine cell death, colonic cells from *Ptpn6*^{spin} >> *Cd47*$^{-/-}$ and WT >> *Ptpn6*^{spin} chimeras were isolated, and both immune (CD45$^+$) and nonimmune (CD45$^-$) cells were analyzed by flow cytometry (fig. S9A). Analysis of CD45$^+$ colonic immune cells by annexin V/propidium iodide (PI) stain showed that annexin V$^+$PI$^+$ populations were increased in *Ptpn6*^{spin} >> *Cd47*$^{-/-}$ mice when compared to WT >> *Ptpn6*^{spin} mice (Fig. 7E). Similar to these results, cell death measured by Ghost Dye (*34*) to examine cell death showed significantly increased CD45$^+$ colonic cell death in *Ptpn6*^{spin} >> *Cd47*$^{-/-}$ mice (Fig. 7F). Analysis of CD45$^-$ nonimmune colonic cells for cell death showed that both annexin$^-$PI$^+$ (necrotic cells) and Ghost Dye$^+$ cells were significantly increased in *Ptpn6*^{spin} >> *Cd47*$^{-/-}$ mice when compared to WT >> *Ptpn6*^{spin} mice (Fig. 7, G and H). In addition to colonic tissues, splenocytes from *Ptpn6*^{spin} >> *Cd47*$^{-/-}$ mice also showed significantly higher level of cell death as demonstrated by increased annexin V$^+$PI$^+$ cells (fig. S9, B and C). Likewise, splenocytes from *Ptpn6*$^{\Delta PMN}$ >> *Cd47*$^{-/-}$ chimeras had increased cell death when compared to *Ptpn6*$^{\Delta PMN}$ >> WT chimeras (fig. S9D). Given that a 1:1 mix bone marrow transfer of WT and *Ptpn6*^{spin} cells into *Cd47*$^{-/-}$ mice also promotes morbidity and mortality (Fig. 6), cell death was examined in these mixed chimeras as well. As expected, increased splenic and colonic (CD45$^+$ and CD45$^-$) cell death was observed in WT + *Ptpn6*^{spin} (1:1) >> *Cd47*$^{-/-}$ chimeras when compared to WT + *Ptpn6*^{spin} (1:1) >> WT chimeras (fig. S10). Together, our data suggest that *Ptpn6*^{spin} bone marrow cells, when transferred to lethally irradiated *Cd47*$^{-/-}$ mice, promote excessive cell death of both immune and nonimmune cells.

Next, to determine gut leakage in *Ptpn6*^{spin} >> *Cd47*$^{-/-}$ chimeras, we performed oral gavage of fluorescein isothiocyanate (FITC)–dextran and analyzed FITC-dextran that leaked into the blood (Fig. 8A). Baseline was determined by measuring leaked FITC-dextran in the serum of WT mice following FITC-dextran oral gavage. The levels of FITC-dextran detected in the serum of WT >> *Cd47*$^{-/-}$ chimeras were like those observed in WT mice (Fig. 8B). In contrast, significantly higher levels of FITC-dextran were detected in the serum of *Ptpn6*^{spin} >> *Cd47*$^{-/-}$ chimeras (Fig. 8B). These data together suggest that loss of gut barrier integrity in *Ptpn6*^{spin} >> *Cd47*$^{-/-}$ chimeras promotes leakage of gut microbes, which may contribute to the morbidity and mortality observed in these mice. Given that lipopolysaccharide (LPS) is a dominant pathogen-associated molecular pattern present in Gram-negative gut microbes (*35*), we injected WT mice with a low dose of LPS intraperitoneally to assess changes in cellular populations. A single challenge with LPS provoked a profound change in WT mice that mimicked cellular changes observed in *Ptpn6*^{spin} >> *Cd47*$^{-/-}$ chimeras (Fig. 8, C and D). Specifically, peripheral blood lymphocyte (PBL) from LPS-challenged WT mice showed marked lymphopenia (reduction in T and B cell populations) and subsequent increase in neutrophils compared to unchallenged WT controls (Fig. 8, C and D).

SIRPα blockade in *Ptpn6*^{spin} >> WT chimeras does not recapitulate lethality observed in *Ptpn6*^{spin} >> *Cd47*$^{-/-}$ chimeras

SIRPα is one of the major counterreceptor for CD47, which is highly expressed on phagocytes (*36*, *37*). Engagement of SIRPα by CD47 has been shown to promote a don't eat me signal to the SIRPα-expressing phagocytes via recruitment of SHP1 and SHP2 to the cyto-tail of SIRPα (*36*, *37*). We first examined the expression of both CD47 and SIRPα on several immune cells in the PBL of WT C57BL/6 mice. Both CD47 and SIRPα were highly expressed on CD11b$^+$Ly6G$^-$ monocytes and CD11b$^+$Ly6G$^+$ neutrophils (fig. S11, A and B). Next, we compared the expression of CD47 and SIRPα in the PBL from WT B6, *Cd47*$^{-/-}$, and *Ptpn6*$^{\Delta PMN}$ mice. The frequency of CD47$^+$ and SIRPα$^+$ cells in the PBL was similar in B6 and *Ptpn6*$^{\Delta PMN}$ mice (fig. S11C). In addition, the expression

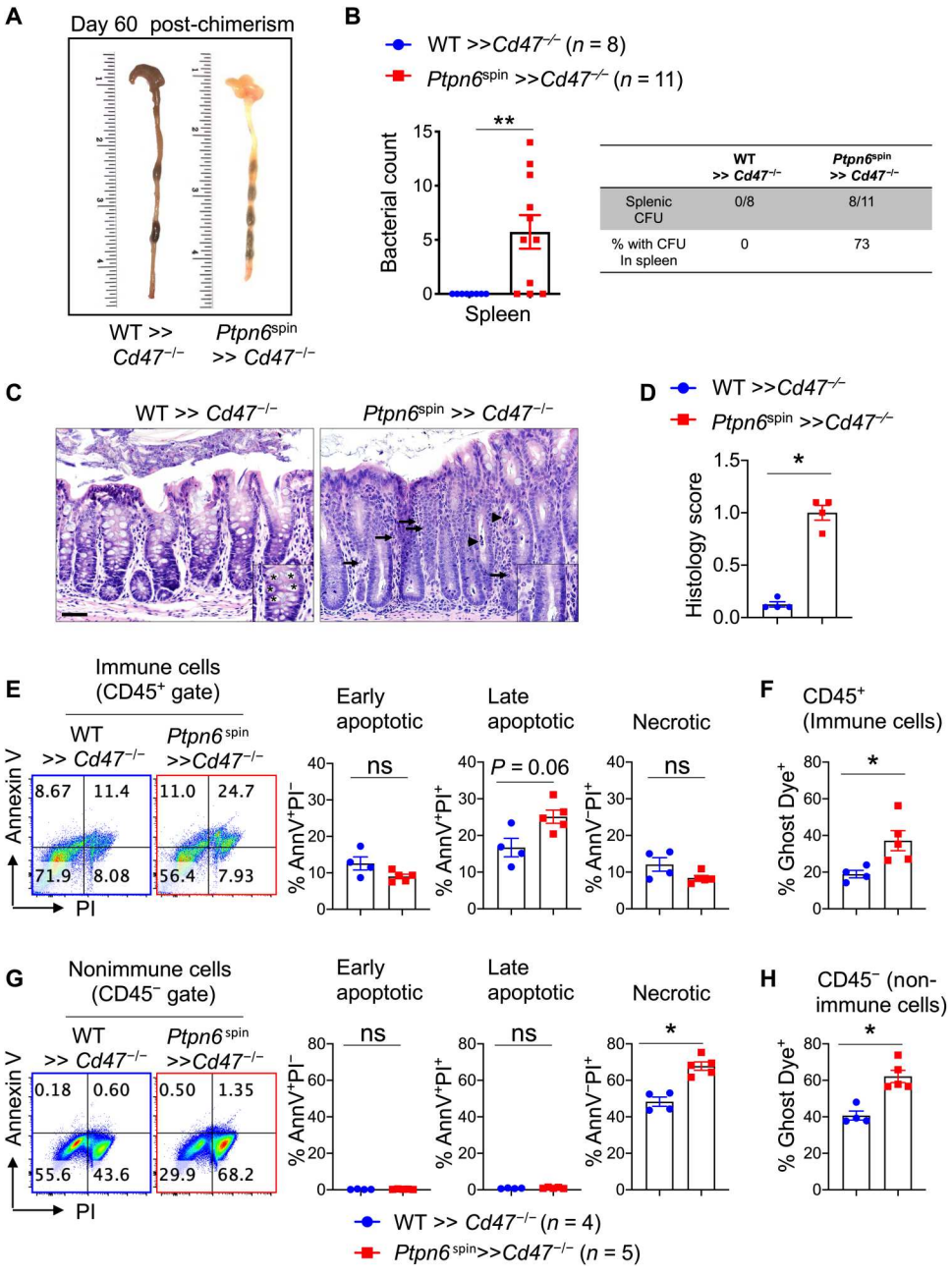

Fig. 7. Increased cell death in *Ptpn6*^{spin} >> *Cd47*$^{-/-}$ mice. (**A**) Whole colon and cecum from *Ptpn6*^{spin} >> *Cd47*$^{-/-}$ mice compared to WT >> *Cd47*$^{-/-}$ mice. (**B**) Bacterial colony count on LB agar plates from spleen lysates of WT >> *Cd47*$^{-/-}$ and *Ptpn6*^{spin} >> *Cd47*$^{-/-}$ chimera mice on day 60 after chimerism. (**C**) Representative intestinal histopathology of WT >> *Cd47*$^{-/-}$ and *Ptpn6*^{spin} >> *Cd47*$^{-/-}$ chimera, H&E stains; scale bar, 55 μm. *Ptpn6*^{spin} >> *Cd47*$^{-/-}$ chimera had more evidence of inflammation characterized by more neutrophilic infiltration (arrows), crypt micro-abscesses (arrowheads), and loss of goblet cells (*insets). (**D**) Scoring of intestinal inflammation represented as histology score. (**E**) Annexin and PI staining of CD45$^+$ immune cells from colon of WT >> *Cd47*$^{-/-}$ and *Ptpn6*^{spin} >> *Cd47*$^{-/-}$ chimera. Annexin V$^+$ and PI$^-$ cells were denoted as early apoptotic, annexin V$^+$PI$^+$ as late apoptotic, and annexin V$^-$PI$^+$ cells as necrotic. (**F**) Ghost Dye staining of CD45$^+$ immune cells from colons of WT >> *Cd47*$^{-/-}$ and *Ptpn6*^{spin} >> *Cd47*$^{-/-}$ chimeras. (**G**) Annexin and PI staining of CD45$^-$ nonimmune cells from colons of WT >> *Cd47*$^{-/-}$ and *Ptpn6*^{spin} >> *Cd47*$^{-/-}$ chimeras. (**H**) Ghost Dye staining of CD45$^-$ nonimmune cells from colons of WT >> *Cd47*$^{-/-}$ and *Ptpn6*^{spin} >> *Cd47*$^{-/-}$ chimeras. Data are means ± SEM. Statistical significance was determined using Mann-Whitney *t* tests. *P* values less than 0.05 were considered statistically significant. *$P \leq 0.05$ and **$P \leq 0.01$.

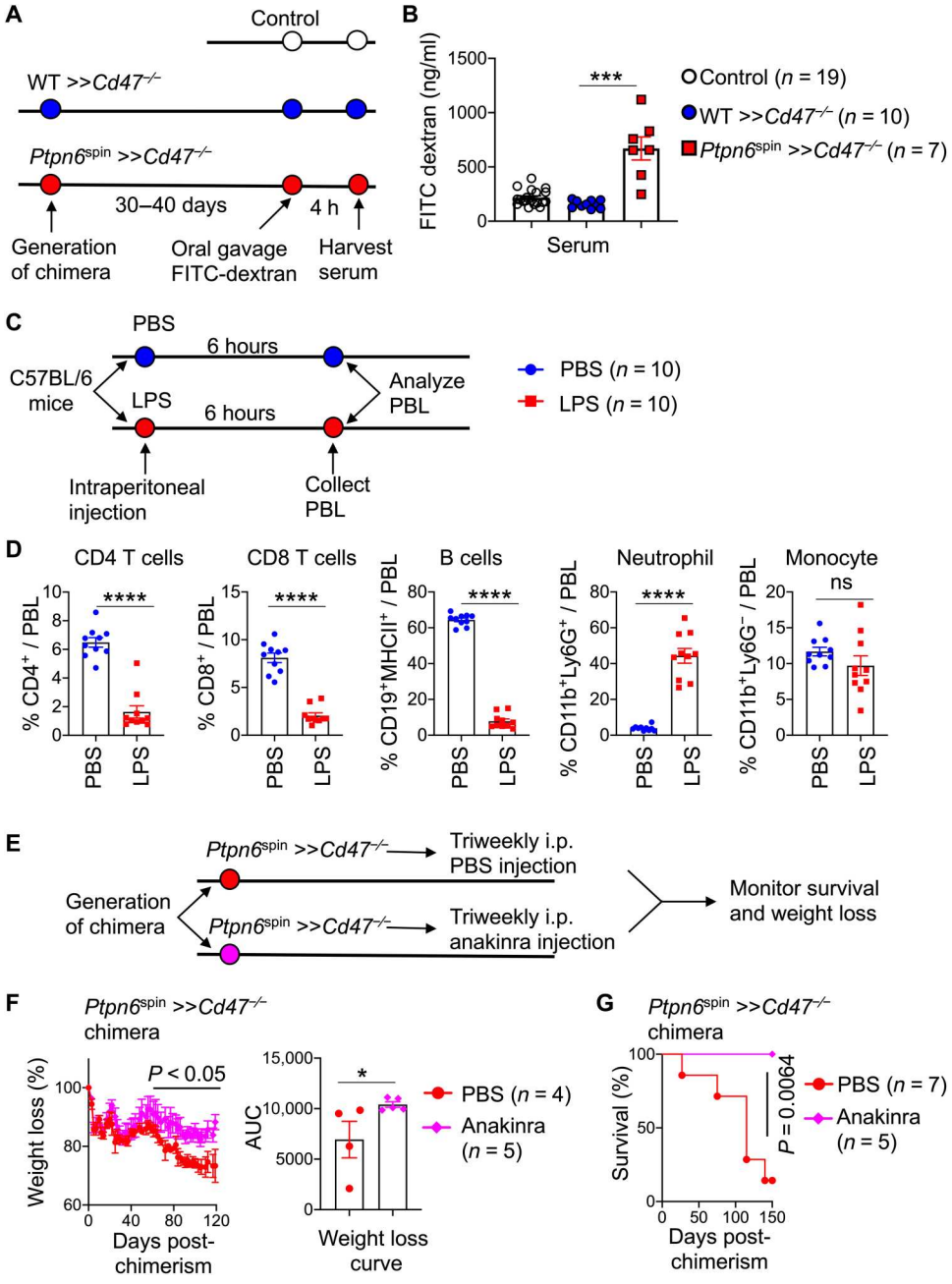

Fig. 8. *Ptpn6*^{spin} >> *Cd47*$^{-/-}$ mice have compromised gut barrier integrity. (**A**) Experimental design for FITC-dextran oral gavage to test gut barrier integrity in WT >> *Cd47*$^{-/-}$ and *Ptpn6*^{spin} >> *Cd47*$^{-/-}$ chimera mice. (**B**) Levels of FITC-dextran detected in the serum of *Ptpn6*^{spin} >> *Cd47*$^{-/-}$ chimeras compared to WT >> *Cd47*$^{-/-}$ chimera and control C57BL/6 WT mice. (**C**) Outline of experimental design. Six- to 8-week-old mice were challenged with PBS or LPS (5 μg per mouse) intraperitoneally. PBL was collected after 24 hours and examined using flow cytometry. (**D**) Frequency of $CD4^+$ T cell, $CD8^+$ T cell, $CD19^+$ B cell, $CD11b^+Ly6G^+$ neutrophil, and $CD11b^+Ly6G^-$ monocyte in the PBL 1 day after LPS challenge. (**E**) Experimental layout for anakinra treatment of *Ptpn6*^{spin} >> *Cd47*$^{-/-}$ chimeras. *Ptpn6*^{spin} >> *Cd47*$^{-/-}$ chimeras were treated with PBS or 400 μg per mouse anakinra three times weekly throughout the course of the study. (**F**) Percent weight loss (left) and AUC (right) of *Ptpn6*^{spin} >> *Cd47*$^{-/-}$ chimeras treated with PBS or anakinra. (**G**) Survival curve of *Ptpn6*^{spin} >> *Cd47*$^{-/-}$ chimeras treated with PBS or anakinra. Each dot represents an individual mouse. Data are means ± SEM. Statistical significance was determined using Mann-Whitney *t* tests for comparing two groups and one-way analysis of variance (ANOVA) for comparing three groups. *P* values less than 0.05 were considered statistically significant. *$P \leq 0.05$, ***$P \leq 0.001$, and ***$P \leq 0.0001$.

of CD47 and SIRPα on neutrophils from B6 and *Ptpn6*$^{\Delta PMN}$ mice was also similar with no notable differences (fig. S11D). These data suggest that *Ptpn6*-deficient neutrophils are not defective in their ability to express CD47 or SIRPα.

To test the hypothesis that CD47 engagement of SIRPα on disease-causing *Ptpn6*^{spin} cells is important to limit the lethal disease, we designed an experiment whereby *Ptpn6*^{spin} >> B6 chimeras were treated with anti-SIRPα antibody to block CD47-SIRPα signaling (fig. S11E). As expected, *Ptpn6*^{spin} >> *Cd47*$^{-/-}$ chimeras started dying around 3 weeks, and all mice died by day 120 (fig. S11E). In contrast, all isotype control or anti-SIRPα antibody–treated *Ptpn6*^{spin} >> B6 chimeras survived the course of the study (fig. S11E). These data suggest that CD47-SIRPα interaction may not be important or that other redundant pathways are present, with TSP1 being a potential candidate (*38*).

Ptpn6^{spin} neutrophils exhibit increased phagocytic potential, which is negatively regulated by CD47

To directly assess the phagocytic ability of WT B6 versus *Ptpn6*^{spin} neutrophils, we used carboxyfluorescein diacetate succinimidyl ester (CFSE)–labeled irradiated splenocytes as a source of target cells. Our results show that compared to B6 neutrophils, a higher frequency of *Ptpn6*^{spin} neutrophils phagocytoses CFSE-labeled B6 splenocytes, specifically at early time points (fig. S12A, row 1 versus row 3). In this same setting, we further examined the phagocytic potential of WT B6 and *Ptpn6*^{spin} neutrophils when exposed to CFSE-labeled irradiated *Cd47*$^{-/-}$ splenocytes. Both WT B6 and *Ptpn6*^{spin} neutrophils phagocytosed more irradiated *Cd47*$^{-/-}$ splenocytes compared to irradiated B6 splenocytes (fig. S12A, row 1 versus row 2, and row 3 versus row 4). Furthermore, *Ptpn6*^{spin} neutrophils phagocytosed more CFSE-labeled irradiated *Cd47*$^{-/-}$ splenocytes when compared to WT B6 neutrophils, which was apparent at 15 min (fig. S12A, row 2 versus row 4).

To further investigate the phagocytic and killing potential of neutrophils, we incubated WT B6 and *Ptpn6*^{spin} neutrophils with green fluorescent protein (GFP)–labeled *Staphylococcus aureus* and examined their phagocytosis followed by intracellular killing over time (fig. S12, A to C). Compared to WT B6 neutrophils, *Ptpn6*^{spin} neutrophils were able to phagocytose higher amount of *S. aureus*, which was evident at early time points (fig. S12B). To examine killing potential, we added gentamicin at 30 min to kill extracellular *S. aureus* and then followed intracellular *S. aureus* within the neutrophils over time. Although *Ptpn6*^{spin} neutrophils phagocytosed a lot more *S. aureus* on a per-cell basis (as demonstrated by mean fluorescence intensity of *S. aureus* in neutrophils), *Ptpn6*^{spin} neutrophils were able to clear the bacteria as fast as the WT neutrophils (fig. S12C). These data together demonstrate that *Ptpn6*^{spin} neutrophils have increased phagocytic and killing potential, and the phagocytic potential is increased by the absence of CD47 on target cells.

IL-1 signaling promotes morbidity and mortality in *Ptpn6*^{spin} >> *Cd47*$^{-/-}$ chimeras

Spontaneous footpad inflammation observed in *Ptpn6*^{spin} mice is provoked by IL-1 signaling since *Ptpn6*^{spin} × *Il1r*$^{-/-}$ mice are completely protected from this disease. We have previously shown that IL-1 signaling is important in both the radioresistant and hematopoietic compartments to drive this inflammatory disease in *Ptpn6*^{spin} mice (*12*). Given that *Ptpn6*^{spin} cells drive morbidity and mortality in *Cd47*$^{-/-}$ recipient mice, we examined the role of IL-1 signaling in the morbidity and mortality observed in *Ptpn6*^{spin} >> *Cd47*$^{-/-}$ chimeras. To test this, *Ptpn6*^{spin} >> *Cd47*$^{-/-}$ chimeras were generated and treated tri-weekly with anakinra (IL-1R antagonist) or phosphate-buffered saline (PBS; control) (Fig. 8E). Our data show that anakinra-treated groups lost significantly less weight compared to PBS groups (Fig. 8F). In addition, 100% of the anakinra-treated *Ptpn6*^{spin} >> *Cd47*$^{-/-}$ chimeras survived, whereas most of the PBS mice died (Fig. 8G). Thus, the morbidity and mortality observed in the *Ptpn6*^{spin} >> *Cd47*$^{-/-}$ chimeras are in part mediated by IL-1 signaling, and blocking IL-1 signaling can mitigate these symptoms.

DISCUSSION

Our study provides a central role for radioresistant CD47 in preventing fatal autoinflammatory disease in *Ptpn6*^{spin} mice. When transferred into lethally irradiated *Cd47*-deficient mice, *Ptpn6*-sufficient (WT) bone marrow cells do not promote observable pathology. In contrast, transfer of *Ptpn6*^{spin} bone marrow cells into a *Cd47*-deficient mouse causes severe wasting syndrome and eventual death. Given that most of these mice survive well beyond 1 month after radiation, we do not believe that these mice are dying of hematopoietic failure, i.e., inability of *Ptpn6*^{spin} bone marrow to fully reconstitute Cd47-deficient recipients. To address this potential issue, 1:1 mixed bone marrow from WT and *Ptpn6*^{spin} mice was transferred into Cd47-deficient mice, which recapitulated the disease observed with transfer of *Ptpn6*^{spin} bone marrow cells alone. *Ptpn6*^{spin} bone marrow cells can fully reconstitute a lethally irradiated WT recipient, although these mice develop an autoinflammatory neutrophilic skin inflammation (*9*, *12*, *16*). Moreover, transfer of bone marrow from *Ptpn6*$^{\Delta myeloid}$ (*Ptpn6* deficiency in myeloid cells) or *Ptpn6*$^{\Delta PMN}$ (*Ptpn6* deficiency in neutrophils) mice into *Cd47*-deficient mice recapitulates fatal wasting syndrome. Because *Ptpn6* deficiency in neutrophils is sufficient and central for provoking fatal disease in CD47-deficient mice, we argue that this disease is an autoinflammatory syndrome; however, it is possible that adaptive cells contribute to the disease downstream of neutrophils.

CD47 is a ubiquitously expressed protein that provides a don't eat me signal to the host phagocytic cells, including neutrophils and macrophages (*37*). Cancer cells have taken advantage of this and express high levels of CD47 to evade recognition and killing by host phagocytic cells (*23*, *25*, *37*). In this regard, targeting CD47 using CD47-neutralizing antibodies has provided benefit in several cancer studies (*39*–*42*). In this light, our studies provide a cautionary note demonstrating a pathogenic outcome of CD47 deficiency (or blockade) under conditions where SHP1 is defective. Hypothetically, in cancer-bearing humans with polymorphisms in the *Ptpn6* gene, CD47-neutralizing therapy may not be the best strategy.

Cd47-deficient mice are born at expected Mendelian ratios and are phenotypically normal without any observable defects (*43*). *Ptpn6*^{spin} mice, a model of neutrophilic dermatosis, are also born at expected Mendelian ratio (*7*). *Ptpn6*^{spin} mice do not exhibit any morbidity at birth and only develop footpad lesions at around 6 to 16 weeks of age (*7*, *9*, *11*, *13*–*15*). When *Cd47*$^{-/-}$ and *Ptpn6*^{spin} mice were bred to generate DKO mice, we found that (i) these mice are not born at expected Mendelian ratio, (ii) most of the DKO mice that are born are significantly smaller than their littermates at

weaning and after, and (iii) more than 50% of the DKO pups die within the first 2 to 3 months of birth. There are several important questions that remain regarding these DKO mice that will need further investigation, which include examining the role of CD47 and SHP1 cross-talk in the embryo. *Ptpn6* deficiency in the hematopoietic compartment is sufficient to provoke neutrophilic footpad inflammation, as demonstrated by the development of footpad lesions in 100% of *Ptpn6*^{spin} >> WT chimeras (*9*, *12*). As we demonstrated in this study, *Ptpn6*^{spin} cells, when transferred into *Cd47*$^{-/-}$ mice (*Ptpn6*^{spin} >> *Cd47*$^{-/-}$ chimeras), develop a systemic inflammatory disease that result in the death of chimera mice. In addition, *Ptpn6*^{spin} bone marrow cells also provoke footpad inflammation in most recipient mice, although the footpad inflammation seemed to dissipate away in some mice when the systemic disease took over. Of note, transfer of bone marrow cells from *Ptpn6*$^{\Delta PMN}$ mice to *Cd47*$^{-/-}$ recipients (*Ptpn6*$^{\Delta PMN}$ >> *Cd47*$^{-/-}$ chimeras) resulted in 100% of chimeras developing severe footpad inflammation. In addition to footpad inflammation, 60% of these mice also had severe tail pathology. Together, these results suggest that CD47 in the radioresistant compartment tempers pathogenic *Ptpn6*^{spin} cells from causing lethal morbidity and mortality.

As shown by several studies, *Ptpn6*^{spin} bone marrow cells transferred into a WT recipient promote neutrophilic dermatosis, which is associated with systemic inflammation hallmarked by splenomegaly (*9*, *12*). In contrast, in addition to neutrophilic dermatosis, *Ptpn6*^{spin} bone marrow cells transferred to *Cd47*-deficient recipients cause significant morbidity and mortality. Thus, we expected massive splenomegaly in *Ptpn6*^{spin} >> *Cd47*$^{-/-}$ chimeras as the disease in these chimera mice is more severe compared to *Ptpn6*^{spin} >> WT chimeras. In contrast, *Ptpn6*^{spin} >> *Cd47*$^{-/-}$ chimeras had significantly smaller spleens that corresponded with reduced splenocyte numbers. Despite having smaller spleens, the splenic immune cell population from *Ptpn6*^{spin} >> *Cd47*$^{-/-}$ chimeras is highly activated, suggesting systemic inflammation in these mice. Further analysis showed that *Ptpn6*^{spin} >> *Cd47*$^{-/-}$ chimera mice exhibit compromised gut barrier integrity that resulted in leakage of gut microbes. We were able to grow several bacterial colonies from the spleen of 8 of 11 *Ptpn6*^{spin} >> *Cd47*$^{-/-}$ chimeras (Fig. 7B). There are several possibilities to why the penetrance was not 100%, given that 100% of these chimeras eventually die: (i) The disease is not synchronous, and hence, mice that have yet to develop lethal disease may not have any gut leakage and (ii) TSB plates used to grow the spleen lysates is not permissive to all gut bacteria, including most of the anaerobes. Our data show increased gut leakage, and given that the gut harbors most of our commensal microbes, we are confident that gut is the likely source of our bacterial colonies found in the spleen of these *Ptpn6*^{spin} >> *Cd47*$^{-/-}$ chimeras. However, we cannot exclude the possibility that some of these bacteria may have come from the lungs, as lungs are also inflamed in these chimeras. We reasoned that this leakage of bacterial products promotes sepsis, which is associated with wasting syndrome, like what is observed in *Ptpn6*^{spin} >> *Cd47*$^{-/-}$ chimeras. Treatment of WT mice with purified endotoxin causes acute changes in immune populations that mimic observations in *Ptpn6*^{spin} >> *Cd47*$^{-/-}$ chimeras. The precise events that result in *Ptpn6*^{spin} cells mediating destruction of the gut barrier epithelial cells are yet unknown and will be the focus of our future studies.

Using a reductionist genetic approach, we show that *Ptpn6*-deficient neutrophils are sufficient to promote lethal disease when transferred into a *Cd47*-deficient recipient. How do these neutrophils cause gut tissue damage? Previous studies have shown that the neutrophilic dermatosis observed in *Ptpn6*^{spin} mice are IL-1α driven (*9*). IL-1α produced by the radioresistant compartment signals neutrophils to produce tumor necrosis factor (TNF), which provokes footpad inflammation (*12*). Given the critical role of IL-1α in instigating neutrophilic inflammation in *Ptpn6*^{spin} mice, we proposed that these cytokines may be involved in the morbidity and mortality observed in *Ptpn6*^{spin} >> *Cd47*$^{-/-}$ chimeras as well. To this end, neutralizing IL-1 signaling by anakinra rescued both morbidity and mortality observed in *Ptpn6*^{spin} >> *Cd47*$^{-/-}$ chimeras. Our genetic and chimera studies have shown that *Ptpn6*^{spin} neutrophils target *Cd47*-deficient radioresistant cells to provoke morbidity and mortality. So how do neutrophils mediate such a pathogenic insult on the CD47 lacking radioresistant cells? Given that CD47 engages SIRP1α on phagocytic cells (*44*), it is possible that these signals are required to inhibit a pathogenic neutrophil response. Our results show that *Ptpn6*^{spin} cells have higher phagocytic and killing potential, which is enhanced when target cells lack CD47. However, our experiment also shows that SIRPα blockade is not sufficient to promote lethal disease in *Ptpn6*^{spin} >> WT chimeras. While our SIRPα blocking strategy was robust (200 μg dose^{-1} mouse^{-1}, three times weekly for ~16 weeks), it is very hard to predict the in vivo efficacy of these antibodies, and thus, a negative result is usually hard to interpret. Given these, our future studies will be aimed at generating *Ptpn6*^{spin} mice that lack SIRP1α, and we anticipate that these DKO mice will recapitulate the disease observed in *Ptpn6*^{spin} × *Cd47*$^{-/-}$ DKO mice.

In summary, our studies have uncovered previously unknown signaling axes involving CD47 and SHP1. In mice with hypomorphic SHP1 protein (*Ptpn6*^{spin} mice) or complete deletion of SHP1 within myeloid cell (*Ptpn6*$^{\Delta myeloid}$, *Ptpn6*$^{\Delta PMN}$ mice), CD47 expression is central for controlling aberrant neutrophil responses, maintaining gut barrier integrity and homeostasis, and preventing lethal morbidity and mortality.

MATERIALS AND METHODS

Mice

C57BL/6J mice were purchased from The Jackson Laboratory (Bar Harbor, ME) and maintained under specific pathogen–free conditions in the animal facilities at the University of Iowa. The mice were reared on a 12-hour light/dark cycle at a constant temperature of 22° ± 1°C. *Ptpn6*^{spin} (MMRRC Repository, stock no. 015198-UCD) (*7*), *Ptpn6*$^{fl/fl}$ (Jackson Labs, stock no. 008336) (*45*), *Cd47*$^{-/-}$ (Jackson Labs, stock no. 003173) (*43*), *Lyz2*-Cre (Jackson Labs, stock no. 004781) (*46*), and *S100a8*-Cre (Jackson Labs, stock no. 021614) (*47*) mice have been described previously. *Cd47*$^{-/-}$ × *Ptpn6*^{spin} DKO mice were generated by breeding *Cd47*$^{-/-}$ and *Ptpn6*^{spin} mice. *Ptpn6*$^{\Delta myeloid}$ and *Ptpn6*$^{\Delta PMN}$ mice were generated by breeding *Ptpn6*$^{fl/fl}$ mice with *Lyz2*-Cre and *S100a8*-Cre mice, respectively. All experimental procedures were approved by the Office of Animal Resources of the University of Iowa (Institutional Animal Care and Use Committee, protocol no. 0032004).

Generation of chimeras and tracking of disease

Bone marrow cells from donor mice were obtained by flushing the femur and tibia, as described previously, with slight modifications

(*48*). Briefly, bone marrows were flushed into a 50-ml conical tube with 5 to 10 ml of sterile PBS using a 23-gauge needle (BD, ref. 305145) and 5-ml syringe (BD, ref. 309646). Once flushed, bone marrow clumps were disrupted using an 18-gauge needle (BD, ref. 305196) and 5-ml syringe. Single-cell suspension of bone marrow cells was filtered through a 40-μm filter, and approximately 5×10^6 cells in 200 μl of PBS were transferred into lethally irradiated (9 Gy) recipient mice via retroorbital sinus injection to generate chimera mice. The chimera mice were weighed one to two times per week and observed for morbidity and mortality.

IL-1 signaling blockade

Ptpn6^{spin} >> *Cd47*$^{-/-}$ chimera mice suffer from systemic inflammatory disease with significant numbers dying following chimerism. To examine the role of IL-1 signaling, *Ptpn6*^{spin} >> *Cd47*$^{-/-}$ chimera mice were treated with tri-weekly intraperitoneal injections of anakinra (400 μg/100 μl per mouse) (IL-1 receptor antagonist, Kiniret, Sobi, NDC 66658-234-07, Stockholm, Sweden) for the length of the study. Chimera mice were weighed one to two times per week and observed for morbidity and mortality.

SIRPα blockade

Ptpn6^{spin} >> WT chimera mice were treated tri-weekly with intraperitoneal injections of anti-SIRPα antibody (200 μg per mouse; *InVivo*Mab anti-mouse CD172a, clone-P84, catalog no. BE0322, Bio X Cell) from days 0 to 110 after chimerism. *Ptpn6*^{spin} >> WT chimera mice treated with Isotype immunoglobulin G (IgG) (Ms IgG Isotype control, lot no. TK2676917, Invitrogen) were used as control. Chimera mice were weighed one to two times per week and monitored for morbidity and mortality.

Whole-body necropsy and histology

All tissues were fixed (10% neutral-buffered formalin, ~4 days), dehydrated through a series of progressive alcohols and xylene, paraffin-embedded, and sectioned at ~4 μm onto glass slides. Tissues were evaluated by a board-certified veterinary pathologist using the post-examination method of evaluation and scoring (*49*). Scoring of intestinal inflammation was performed as previous described (*50*). Briefly, an H score was calculated using the following scale: 0, lack of lesions; 1, mild, scattered leukocyte infiltration in lamina propria, increased height of proliferating crypts; 2, moderate, multifocal aggregates of infiltrating leukocytes in lamina propria extending into the submucosa, increased height, and proliferation of mucosa with loss of goblet cells, crypt abscesses detectable; 3, severe, coalescing aggregates of infiltrating leukocytes expanding lamina propria and submucosa with evidence of crypt dropout. A composite tissue score (histology score) was made for each tissue by dividing the H score by 100.

Flow cytometry analysis

Flow cytometry analysis was performed in splenocytes and PBL.

Splenocyte preparation: Single-cell suspension of splenocytes was acquired by grinding the spleen with the back end of a 3-ml syringe plunger (BD, ref. 309657) and passing the cells through a 70-μm cell strainer. Red blood cells (RBCs) in the splenocytes were lysed using RBC lysis buffer [ammonium chloride lysis buffer: NH_4Cl 0.802 g, $NaHCO_3$, 0.84 g, and Ethylenediaminetetraacetic acid (EDTA) 0.37 g]. RBC-free splenocytes were resuspended in fluorescence-activated cell sorting (FACS) buffer [PBS, 2% fetal bovine serum (FBS; R&D Systems, catalog no. 511150), 1 mM EDTA, and 0.1% sodium azide], counted using a hemocytometer, and prepared for surface staining.

PBL preparation: Blood samples (100 μl) were collected from retroorbital sinuses using calibrated pipettes (Drummond Scientific Company, Broomall, PA, catalog no. 2-000-100) into 1.5-ml microcentrifuge tubes. RBCs were lysed using RBC lysis buffer. The RBC lysis step was repeated two times to ensure that all RBCs were lysed. Following complete RBC lysis, cells were resuspended in FACS buffer and prepared for surface staining.

Colon preparation: Full-length colonic tissues were harvested. Fecal pellets in the colon were pushed out using forceps, and colon was washed using 2 to 3 ml of PBS. Colons were cut longitudinally to open the lumen and further cut into 8 to 10 small pieces (~1 mm) and placed in 50-ml conical tube with 20 ml of cold wash buffer [500 ml of 1× Hanks′ balanced salt solution (Gibco, ref. 14175-595) + 25 ml of 1 M Hepes (Gibco, ref. 15630-080) + 10 ml of FBS]. Colon pieces were washed three times with wash buffer, transferred into a 10-cm petri dish, and cut into small pieces. Chopped pieces were transferred to a 15-ml conical tube, resuspended in 5 ml of collagenase buffer [RPMI 1640 + 10% FBS + collagenase-1 (1 mg/ml; Gibco, ref. 11875-093)], and incubated at 37°C in a shaking incubator. After 1 hour, digested tissue and buffer were transferred to a 50-ml conical tube straining through a 70-mm mesh strainer (Falcon, NC, ref. 325350). Leftover tissues on the strainer were macerated using the plunger end of a 3-ml syringe and rinsed with 10 ml of PBS. Cells were centrifuged at 1000*g* for 10 min, resuspended in FACS buffer, and prepared for surface staining.

Flow cytometry staining and analysis: Single-cell suspensions of splenocytes and PBL were stained using different fluorochrome-conjugated antibodies, as described previously (*51*). Anti-mouse CD8 [brilliant violet (BV) 605, clone 53-6.7, BD Biosciences, San Jose, CA], anti-mouse CD4 (BV786, clone GK 1.5, BD Biosciences), anti-mouse CD44 (BV421, clone 1 M7, BD Biosciences), anti-mouse CD3e [phycoerythrin (PE)–cyanine 7, clone 145-2C11, TONBO Biosciences, San Diego, CA], anti-mouse CD11a antibody (FITC conjugate, clone M17/4, TONBO Biosciences), anti-mouse Ly-6G (violet flour 450, clone 1A8, TONBO Biosciences), anti-mouse CD19 (PE-cyanine 7, clone 1D3, TONBO Biosciences), anti-mouse MHC class II (I/A/ I-E) (PE, clone M5/114-15.2, TONBO Biosciences), anti-human/mouse CD11b (FITC, clone M1/70, TONBO Biosciences), and anti-mouse CD11c (BV510, clone HL3, BD Biosciences) were used for staining of cells. For cell death analysis, single-cell suspension of splenocytes and PBL was stained with annexin V and PI using an annexin V-FITC apoptosis kit (lot 7D07K01010, BioVision, Milpitas, CA) or alternatively stained with Ghost Dye (Violet450, ref. 13-0863/Violet510, ref. 13-0870, TONBO Biosciences).

Stained samples were run on a flow cytometer (Cytoflex, Beckman Coulter, IN), and raw data were analyzed using FlowJo 10 software (FlowJo LLC, Ashland, OR).

Bacterial culture

Spleens were homogenized in 1 ml of PBS, and 20 μl of the homogenized spleen lysates was plated on TSB agar plates and incubated at 37°C overnight to determine numbers of colony-forming units.

In vitro phagocytosis assay

GFP–S. aureus culture

GFP-expressing *S. aureus* (1 μl; USA 300 strain) from a frozen stock was inoculated into 5 ml of sterile LB broth in a 15-ml conical tube. The tube was loosely capped and transferred in the 37°C incubator on a shaker at 200 rpm overnight. The next day, fresh 5 ml of LB broth was inoculated with 0.5 ml of overnight culture. The optical density (OD) was measured and used for phagocytosis assay when it was between 0.5 and 1 at OD_{600}.

Neutrophil isolation from bone marrow using Histopaque

Bone marrow cells were isolated as described previously in Materials and Methods for generation of chimeras. Single-cell suspension of bone marrow cells was filtered through a 40-μm filter and resuspended in complete RPMI 1640 medium. Neutrophils were isolated from bone marrow using Histopaque gradient layering. Briefly, 3 ml of Histopaque 1119 (density, 1.119 g/ml; lot no. RNBK3107, Sigma-Aldrich) was added in 15-ml conical tube, which was then overlaid with Histopaque 1077 (density, 1.077 g/ml; RNBK4517, Sigma-Aldrich). Single-cell suspension (1 ml) of bone marrow cells was overlaid on top of Histopaque 1077 layer and centrifuged for 30 min at 872*g* at room temperature without brakes. The neutrophil at the interface of the Histopaque 1119 and Histopaque 1077 layers was carefully collected and transferred to 15-ml conical tube. Collected neutrophils were washed twice with complete RPMI 1640 medium at 1400 rpm for 5 min at 4°C. Small aliquot was taken to determine the neutrophil count using trypan blue exclusion, and purity was determined using flow cytometry.

CFSE labeling of splenocytes and irradiation

Isolated splenocytes were incubated with 3 μM CFSE proliferation dye (ref. no. 13-0850-U500, TONBO) for 5 min at 37°C in the dark. CFSE labeling was quenched by adding an equal volume of FBS for 5 min at room temperature. Then, the cells were washed twice with FACS buffer and resuspended in 2 ml of complete RPMI 1640 medium. Splenocyte count was determined using trypan blue. CFSE-stained splenocytes were irradiated with 40 Gy of cesium to use as a source of target cells for neutrophil phagocytosis assay.

Phagocytosis assay

CFSE-labeled irradiated splenocytes (100 μl of 20×10^6/ml; WT or *CD47*$^{-/-}$) were added to 96-well plate seeded with 100 μl of 2×10^6/ml of neutrophils (WT and *Ptpn6*^{spin}) (1:10 ratio). The culture plate was incubated at 37°C, and samples were collected at different time points. The phagocytosis was determined using flow cytometry by measuring $CFSE^+$ neutrophils.

GFP-expressing *S. aureus* (multiplicity of infection, 5) was added to neutrophils (100 μl of 1×10^6/ml) in a 96-well plate to determine bacterial phagocytosis. The culture plate was incubated at 37°C, and samples collected at different time points. Gentamicin (lot no. 16F065301, IBI Scientific, Peosta, IA) was added at 50 μg/ml to the culture to kill extracellular *S. aureus* at 30 min. The phagocytosis was determined using flow cytometry by measuring GFP^+ neutrophils.

FITC-dextran oral gavage

Intestinal barrier integrity was determined as demonstrated previously (*52*). Briefly, to assess intestinal barrier integrity, FITC-dextran (FD4, Sigma-Aldrich, St. Louis, MO) was introduced via oral gavage. Mice were deprived of water for 4 hours and then administered FITC-dextran (44 mg/100 g body weight) at a concentration of 100 mg/ml in PBS. Mice were then sacrificed with CO_2 inhalation, blood was collected via cardiac puncture, and serum was isolated with BD Microtainer SST tubes (365968, BD Bioscience) following the manufacturer's instructions. For analysis, a standard curve was established with serially diluted FITC-dextran and compared to a sample containing an equal volume of serum and PBS. Serum was also collected from mice receiving no FITC-dextran as background control. Using a 96-well plate, samples were assessed spectrophotofluorometrically with an excitation wavelength of 485 nm and an emission wavelength of 528 nm.

Bacterial LPS challenge

Eight-week-old C57BL/6 mice were injected with PBS or LPS (5 mg/kg) intraperitoneally. Six hours after LPS injection, PBL was collected and analyzed for frequency of leukocyte populations by flow cytometry.

Statistical analysis

Statistical analysis was performed, and figures were generated using GraphPad Prism 8.0 software. Statistical significance was determined using Mann-Whitney *t* tests for two groups and one-way analysis of variance (ANOVA) (with Dunnett's or Tukey's multiple comparisons tests) for three or more groups. All values are expressed as means ± SEM. Disease-free and survival curve analyses were done using the log-rank (Mantel-Cox) test. $P < 0.05$ was considered statistically significant.

Supplementary Materials

This PDF file includes:

Figs. S1 to S12

View/request a protocol for this paper from *Bio-protocol*.

REFERENCES AND NOTES

1. P. R. Cohen, Sweet's syndrome—A comprehensive review of an acute febrile neutrophilic dermatosis. *Orphanet J. Rare Dis.* **2**, 34 (2007).
2. P. J. Watts, A. Khachemoune, Subcorneal pustular dermatosis: A review of 30 years of progress. *Am. J. Clin. Dermatol.* **17**, 653–671 (2016).
3. A. Alavi, L. E. French, M. D. Davis, A. Brassard, R. S. Kirsner, Pyoderma gangrenosum: An update on pathophysiology, diagnosis and treatment. *Am. J. Clin. Dermatol.* **18**, 355–372 (2017).
4. A. Filosa, G. Filosa, Neutrophilic dermatoses: A broad spectrum of disease. *G. Ital. Dermatol. Venereol.* **153**, 265–272 (2018).
5. P. R. Cohen, Neutrophilic dermatoses: A review of current treatment options. *Am. J. Clin. Dermatol.* **10**, 301–312 (2009).
6. A. B. Nesterovitch, Z. Gyorfy, M. D. Hoffman, E. C. Moore, N. Elbuluk, B. Tryniszewska, T. A. Rauch, M. Simon, S. Kang, G. J. Fisher, K. Mikecz, M. D. Tharp, T. T. Glant, Alteration in the gene encoding protein tyrosine phosphatase nonreceptor type 6 (PTPN6/SHP1) may contribute to neutrophilic dermatoses. *Am. J. Pathol.* **178**, 1434–1441 (2011).
7. B. A. Croker, B. R. Lawson, S. Rutschmann, M. Berger, C. Eidenschenk, A. L. Blasius, E. M. Moresco, S. Sovath, L. Cengia, L. D. Shultz, A. N. Theofilopoulos, S. Pettersson, B. A. Beutler, Inflammation and autoimmunity caused by a SHP1 mutation depend on IL-1, MyD88, and a microbial trigger. *Proc. Natl. Acad. Sci. U.S.A.* **105**, 15028–15033 (2008).
8. A. B. Nesterovitch, S. Szanto, A. Gonda, T. Bardos, K. Kis-Toth, V. A. Adarichev, K. Olasz, S. Ghassemi-Najad, M. D. Hoffman, M. D. Tharp, K. Mikecz, T. T. Glant, Spontaneous insertion of a b2 element in the ptpn6 gene drives a systemic autoinflammatory disease in mice resembling neutrophilic dermatosis in humans. *Am. J. Pathol.* **178**, 1701–1714 (2011).
9. J. R. Lukens, P. Vogel, G. R. Johnson, M. A. Kelliher, Y. Iwakura, M. Lamkanfi, T. D. Kanneganti, RIP1-driven autoinflammation targets IL-1α independently of inflammasomes and RIP3. *Nature* **498**, 224–227 (2013).
10. C. L. Abram, G. L. Roberge, L. I. Pao, B. G. Neel, C. A. Lowell, Distinct roles for neutrophils and dendritic cells in inflammation and autoimmunity in motheaten mice. *Immunity* **38**, 489–501 (2013).

11. B. A. Croker, R. S. Lewis, J. J. Babon, J. D. Mintern, D. E. Jenne, D. Metcalf, J. G. Zhang, L. H. Cengia, J. A. O'Donnell, A. W. Roberts, Neutrophils require SHP1 to regulate IL-1β production and prevent inflammatory skin disease. *J. Immunol.* **186**, 1131–1139 (2011).
12. P. Gurung, G. Fan, J. R. Lukens, P. Vogel, N. K. Tonks, T. D. Kanneganti, Tyrosine kinase SYK licenses MyD88 adaptor protein to instigate IL-1α-mediated inflammatory disease. *Immunity* **46**, 635–648 (2017).
13. S. Tartey, P. Gurung, T. K. Dasari, A. Burton, T. D. Kanneganti, ASK1/2 signaling promotes inflammation in a mouse model of neutrophilic dermatosis. *J. Clin. Invest.* **128**, 2042–2047 (2018).
14. S. Tartey, P. Gurung, R. Karki, A. Burton, P. Hertzog, T. D. Kanneganti, Ets-2 deletion in myeloid cells attenuates IL-1α-mediated inflammatory disease caused by a *Ptpn6* point mutation. *Cell. Mol. Immunol.* **18**, 1798–1808 (2020).
15. S. Tartey, P. Gurung, P. Samir, A. Burton, T. D. Kanneganti, Cutting edge: Dysregulated CARD9 signaling in neutrophils drives inflammation in a mouse model of neutrophilic dermatoses. *J. Immunol.* **201**, 1639–1644 (2018).
16. P. Gurung, T. D. Kanneganti, Autoinflammatory skin disorders: The inflammasomme in focus. *Trends Mol. Med.* **22**, 545–564 (2016).
17. A. V. Marzano, A. G. Ortega-Loayza, M. Heath, D. Morse, G. Genovese, M. Cugno, Mechanisms of inflammation in neutrophil-mediated skin diseases. *Front. Immunol.* **10**, 1059 (2019).
18. I. Haase, R. M. Hobbs, M. R. Romero, S. Broad, F. M. Watt, A role for mitogen-activated protein kinase activation by integrins in the pathogenesis of psoriasis. *J. Clin. Invest.* **108**, 527–536 (2001).
19. R. M. Hobbs, F. M. Watt, Regulation of interleukin-1α expression by integrins and epidermal growth factor receptor in keratinocytes from a mouse model of inflammatory skin disease. *J. Biol. Chem.* **278**, 19798–19807 (2003).
20. N. C. Di Paolo, E. A. Miao, Y. Iwakura, K. Murali-Krishna, A. Aderem, R. A. Flavell, T. Papayannopoulou, D. M. Shayakhmetov, Virus binding to a plasma membrane receptor triggers interleukin-1 alpha-mediated proinflammatory macrophage response in vivo. *Immunity* **31**, 110–121 (2009).
21. E. J. Brown, W. A. Frazier, Integrin-associated protein (CD47) and its ligands. *Trends Cell Biol.* **11**, 130–135 (2001).
22. A. Russ, A. B. Hua, W. R. Montfort, B. Rahman, I. B. Riaz, M. U. Khalid, J. S. Carew, S. T. Nawrocki, D. Persky, F. Anwer, Blocking "don't eat me" signal of CD47-SIRPα in hematological malignancies, an in-depth review. *Blood Rev.* **32**, 480–489 (2018).
23. S. Jaiswal, C. H. Jamieson, W. W. Pang, C. Y. Park, M. P. Chao, R. Majeti, D. Traver, N. van Rooijen, I. L. Weissman, CD47 is upregulated on circulating hematopoietic stem cells and leukemia cells to avoid phagocytosis. *Cell* **138**, 271–285 (2009).
24. X. Liu, Y. Pu, K. Cron, L. Deng, J. Kline, W. A. Frazier, H. Xu, H. Peng, Y. X. Fu, M. M. Xu, CD47 blockade triggers T cell-mediated destruction of immunogenic tumors. *Nat. Med.* **21**, 1209–1215 (2015).
25. R. Majeti, M. P. Chao, A. A. Alizadeh, W. W. Pang, S. Jaiswal, K. D. Gibbs Jr., N. van Rooijen, I. L. Weissman, CD47 is an adverse prognostic factor and therapeutic antibody target on human acute myeloid leukemia stem cells. *Cell* **138**, 286–299 (2009).
26. H. L. Matlung, K. Szilagyi, N. A. Barclay, T. K. van den Berg, The CD47-SIRPα signaling axis as an innate immune checkpoint in cancer. *Immunol. Rev.* **276**, 145–164 (2017).
27. K. Weiskopf, N. S. Jahchan, P. J. Schnorr, S. Cristea, A. M. Ring, R. L. Maute, A. K. Volkmer, J. P. Volkmer, J. Liu, J. S. Lim, D. Yang, G. Seitz, T. Nguyen, D. Wu, K. Jude, H. Guerston, A. Barkal, F. Trapani, J. George, J. T. Poirier, E. E. Gardner, L. A. Miles, E. de Stanchina, S. M. Lofgren, H. Vogel, M. M. Winslow, C. Dive, R. K. Thomas, C. M. Rudin, M. van de Rijn, R. Majeti, K. C. Garcia, I. L. Weissman, J. Sage, CD47-blocking immunotherapies stimulate macrophage-mediated destruction of small-cell lung cancer. *J. Clin. Invest.* **126**, 2610–2620 (2016).
28. C. K. Brierley, J. Staves, C. Roberts, H. Johnson, P. Vyas, L. T. Goodnough, M. F. Murphy, The effects of monoclonal anti-CD47 on RBCs, compatibility testing, and transfusion requirements in refractory acute myeloid leukemia. *Transfusion* **59**, 2248–2254 (2019).
29. L. D. S. Johnson, S. Banerjee, O. Kruglov, N. N. Viller, S. M. Horwitz, A. Lesokhin, J. Zain, C. Querfeld, R. Chen, C. Okada, A. Sawas, O. A. O'Connor, E. L. Sievers, Y. Shou, R. A. Uger, M. Wong, O. E. Akilov, Targeting CD47 in Sézary syndrome with SIRPαFc. *Blood Adv.* **3**, 1145–1153 (2019).
30. B. I. Sikic, N. Lakhani, A. Patnaik, S. A. Shah, S. R. Chandana, D. Rasco, A. D. Colevas, T. O'Rourke, S. Narayanan, K. Papadopoulos, G. A. Fisher, V. Villalobos, S. S. Prohaska, M. Howard, M. Beeram, M. P. Chao, B. Agoram, J. Y. Chen, J. Huang, M. Axt, J. Liu, J. P. Volkmer, R. Majeti, I. L. Weissman, C. H. Takimoto, D. Supan, H. A. Wakelee, R. Aoki, M. D. Pegram, S. K. Padda, First-in-human, first-in-class phase I trial of the anti-CD47 antibody Hu5F9-G4 in patients with advanced cancers. *J. Clin. Oncol.* **37**, 946–953 (2019).
31. S. M. Lewis, A. Williams, S. C. Eisenbarth, Structure and function of the immune system in the spleen. *Sci. Immunol.* **4**, eaau6085 (2019).
32. C. L. Abram, G. L. Roberge, Y. Hu, C. A. Lowell, Comparative analysis of the efficiency and specificity of myeloid-Cre deleting strains using ROSA-EYFP reporter mice. *J. Immunol. Methods* **408**, 89–100 (2014).
33. M. Speir, C. J. Nowell, A. A. Chen, J. A. O'Donnell, I. S. Shamie, P. R. Lakin, A. A. D'Cruz, R. O. Braun, J. J. Babon, R. S. Lewis, M. Bliss-Moreau, I. Shlomovitz, S. Wang, L. H. Cengia, A. I. Stoica, R. Hakem, M. A. Kelliher, L. A. O'Reilly, H. Patsiouras, K. E. Lawlor, E. Weller, N. E. Lewis, A. W. Roberts, M. Gerlic, B. A. Croker, Ptpn6 inhibits caspase-8- and Ripk3/Mlkl-dependent inflammation. *Nat. Immunol.* **21**, 54–64 (2020).
34. C. H. Poholek, I. Raphael, D. Wu, S. Revu, N. Rittenhouse, U. U. Uche, S. Majumder, L. P. Kane, A. C. Poholek, M. J. McGeachy, Noncanonical STAT3 activity sustains pathogenic Th17 proliferation and cytokine response to antigen. *J. Exp. Med.* **217**, e20191761 (2020).
35. L. Mazgaeen, P. Gurung, Recent advances in lipopolysaccharide recognition systems. *Int. J. Mol. Sci.* **21**, 379 (2020).
36. Y. Murata, T. Kotani, H. Ohnishi, T. Matozaki, The CD47-SIRPα signalling system: Its physiological roles and therapeutic application. *J. Biochem.* **155**, 335–344 (2014).
37. P.-A. Oldenborg, CD47: A cell surface glycoprotein which regulates multiple functions of hematopoietic cells in health and disease. *ISRN Hematol.* **2013**, 614619 (2013).
38. A. Kale, N. M. Rogers, K. Ghimire, Thrombospondin-1 CD47 signalling: From mechanisms to medicine. *Int. J. Mol. Sci.* **22**, 4062 (2021).
39. D. Kim, J. Wang, S. B. Willingham, R. Martin, G. Wernig, I. L. Weissman, Anti-CD47 antibodies promote phagocytosis and inhibit the growth of human myeloma cells. *Leukemia* **26**, 2538–2545 (2012).
40. J. Liu, L. Wang, F. Zhao, S. Tseng, C. Narayanan, L. Shura, S. Willingham, M. Howard, S. Prohaska, J. Volkmer, M. Chao, I. L. Weissman, R. Majeti, Pre-clinical development of a humanized anti-CD47 antibody with anti-cancer therapeutic potential. *PLOS ONE* **10**, e0137345 (2015).
41. X. Zhang, Y. Wang, J. Fan, W. Chen, J. Luan, X. Mei, S. Wang, Y. Li, L. Ye, S. Li, W. Tian, K. Yin, D. Ju, Blocking CD47 efficiently potentiated therapeutic effects of anti-angiogenic therapy in non-small cell lung cancer. *J. Immunother. Cancer* **7**, 346 (2019).
42. W. Zhang, Q. Huang, W. Xiao, Y. Zhao, J. Pi, H. Xu, H. Zhao, J. Xu, C. E. Evans, H. Jin, Advances in anti-tumor treatments targeting the CD47/SIRPα axis. *Front. Immunol.* **11**, 18 (2020).
43. F. P. Lindberg, D. C. Bullard, T. E. Caver, H. D. Gresham, A. L. Beaudet, E. J. Brown, Decreased resistance to bacterial infection and granulocyte defects in IAP-deficient mice. *Science* **274**, 795–798 (1996).
44. T. Matozaki, Y. Murata, H. Okazawa, H. Ohnishi, Functions and molecular mechanisms of the CD47-SIRPα signalling pathway. *Trends Cell Biol.* **19**, 72–80 (2009).
45. L. I. Pao, K. P. Lam, J. M. Henderson, J. L. Kutok, M. Alimzhanov, L. Nitschke, M. L. Thomas, B. G. Neel, K. Rajewsky, B cell-specific deletion of protein-tyrosine phosphatase Shp1 promotes B-1a cell development and causes systemic autoimmunity. *Immunity* **27**, 35–48 (2007).
46. B. E. Clausen, C. Burkhardt, W. Reith, R. Renkawitz, I. Förster, Conditional gene targeting in macrophages and granulocytes using LysMcre mice. *Transgenic Res.* **8**, 265–277 (1999).
47. E. Passegue, E. F. Wagner, I. L. Weissman, JunB deficiency leads to a myeloproliferative disorder arising from hematopoietic stem cells. *Cell* **119**, 431–443 (2004).
48. S. R. Amend, K. C. Valkenburg, K. J. Pienta, Murine hind limb long bone dissection and bone marrow isolation. *J. Vis. Exp.* , 53936 (2016).
49. D. K. Meyerholz, A. P. Beck, Principles and approaches for reproducible scoring of tissue stains in research. *Lab. Invest.* **98**, 844–855 (2018).
50. R. Geesala, W. Schanz, M. Biggs, G. Dixit, J. Skurski, P. Gurung, D. K. Meyerholz, D. Elliott, P. D. Issuree, T. Maretzky, Loss of RHBDF2 results in an early-onset spontaneous murine colitis. *J. Leukoc. Biol.* **105**, 767–781 (2019).
51. P. Gurung, B. R. Sharma, T. D. Kanneganti, Distinct role of IL-1β in instigating disease in *Sharpin*^{cpdm} mice. *Sci. Rep.* **6**, 36634 (2016).
52. J. Gupta, I. del Barco Barrantes, A. Igea, S. Sakellariou, I. S. Pateras, V. G. Gorgoulis, A. R. Nebreda, Dual function of p38α MAPK in colon cancer: Suppression of colitis-associated tumor initiation but requirement for cancer cell survival. *Cancer Cell* **25**, 484–500 (2014).

Acknowledgments: We thank K. Greiner for help with scientific editing. We thank K. Gibson-Corley and the Division of Comparative Pathology in the Department of Pathology for their help with processing of tissue samples. GFP-expressing *S. aureus* (USA300 strain) was a gift from C. Parlet. The content is solely the responsibility of the authors and does not necessarily represent the official views of the National Institutes of Health. **Funding:** This work was supported by the National Institute of Allergy and Infectious Diseases (K22 AI127836, R21 AI148904, and R01 AI155425) and the University of Iowa start-up funds granted to P.G. T.-D.K. is supported by funding from the U.S. National Institutes of Health (AI101935, AI124346, AI160179, AR056296, and CA253095) and the American Lebanese Syrian Associated Charities (ALSAC). **Author contributions:** P.G. and T.-D.K. designed and conceptualized the study. L.M., M.Y., S.S., and P.G. performed experiments. L.M. and P.G. analyzed data with input from other

authors. D.K.M. and P.V. conducted histologic analysis. L.M. and P.G. wrote the manuscript with input from other authors. P.G. oversaw the project. **Competing interests:** T.-D.K. is a consultant for Pfizer. The authors declare no other competing interests. **Data and materials availability:** All data needed to evaluate the conclusions in the paper are present in the paper and/or the Supplementary Materials.

Submitted 13 August 2022
Accepted 1 December 2022
Published 6 January 2023
10.1126/sciadv.ade3942